

POLITECNICO DI TORINO

Dipartimento di Elettronica e Telecomunicazioni

Master Degree in Biomedical Engineering

**Automatic Identification of Spike
and Waves in the EEG of
Epileptic Patients**



Supervisor

Luca Mesin

Candidate

Alberto Faedda

December 2020

Abstract

Reading an EEG by neurologists, to diagnose epilepsy or to evaluate pathological events that contribute to the diagnosis, is very time consuming. A pathological event of the EEG that is indicative of epilepsy is the spike and wave. The objective of the study is the creation of an epileptic spike and waves detector based on a set of matched filters to support the diagnosis of epilepsy through a tool capable of detecting spike and waves in the EEG signal.

The first chapter provides anatomical, biological and physiological information necessary to understand the problem. A brief description of epilepsy and its classifications is also described, with the related pathological waveforms that can be found in the EEG. The second chapter illustrates some mathematical concepts useful for better understanding the work. The third chapter describes the dataset used consisting of 10 EEG signals and the method for identifying the spike and waves from the signals. The results achieved are described in chapter four. In particular, the average true positive rate (TPR) obtained considering all patients is 85%, with an average precision (PPV) of 67%. Then the algorithm was tested to a dataset of healthy patients to understand if it was able to distinguish between healthy and sick patients. It has also been noted that even in patients with attention deficit hyperactivity disorder (ADHD) there is the presence of spike and waves. It has been observed also that the number and frequency of spikes change according to the period considered, showing an increase in the *pre-ictal* period compared to the *inter-ictal* period, with a considerable increase during the seizure. Finally, the last chapter describes some improvements that could be made and future research that could be carried out.

Contents

1	Introduction	11
1.1	Nervous System and EEG	11
1.1.1	Nervous System Anatomy	11
1.1.2	Neurons	12
1.1.3	Nervous System Physiology	13
1.1.4	EEG Signal Characteristics	15
1.1.5	The International 10-20 System	17
1.2	Epilepsy	18
1.2.1	Classification	19
1.2.2	EEG Waveform Abnormalities	20
1.2.3	Spike and Wave	22
1.2.4	Diagnosis and Therapy	22
2	Mathematical Concepts	25
2.1	Blind Source Separation (BSS)	25
2.1.1	Second Order Blind Source Separation	26
2.1.2	Canonical Correlation Analysis	27
2.2	Matched Filtering	28
2.2.1	Wavelet Example	29
3	Materials and Methods	31
3.1	Dataset	31
3.2	Preprocessing	32
3.2.1	EOG Removal	33
3.2.2	EMG Removal	35
3.3	Algorithm	36
3.3.1	Prototype Waveforms Construction	36
3.3.2	Calculation of the Normalized Cross-Correlation	38
4	Results	43
4.1	Evaluation of Algorithm Results	43
4.2	Clinical Applications	45
4.2.1	Comparison With Healthy Patients	45
4.2.2	Comparison With ADHD Patients	47
4.2.3	Temporal and Spatial Distribution	49
5	Conclusions and Future Work	55

List of Figures

1.1 Central and Peripheral Nervous System	12
1.2 Structure of a neuron	12
1.3 Action potential	14
1.4 Brain wave patterns	16
1.5 International 10-20 system	17
1.6 EEG waveform abnormalities	20
2.1 Basic filter structure	29
2.2 First 100 ms of wavelet	29
2.3 Noisy signals and wavelets	30
2.4 Matched filters results	30
3.1 EEG channels distribution	31
3.2 Bode diagram Chebyshev type II highpass filter, order 5	32
3.3 Bode diagram Chebyshev type II lowpass filter, order 6	33
3.4 10 seconds of EEG signal after bandpass filter and before EOG removal	34
3.5 10 seconds of EEG signal after EOG removal	34
3.6 10 seconds of EEG signal after EMG removal	36
3.7 Prototype waveform	37
3.8 Set of prototypes	38
3.9 Absolute value of normalized cross-correlation	40
3.10 Waveforms identified in 20 seconds of original EEG epoch	41
3.11 Spike and wave complex identified by the algorithm	41
4.1 Difference between number of waves per second identified by algorithm	45
4.2 Difference between amplitude distributions	46
4.3 Waveforms identified in ADHD patient	47
4.4 Difference between number of identified waves per second	48
4.5 Difference between amplitude distributions	48
4.6 Times of appearance	49
4.7 Number of identified waves per second in each period	50
4.8 Distribution in each period	50
4.9 Distribution over the scalp in each period	51
4.10 Number of identified waves per second in each period (Boxplot)	52
4.11 Mean time interval variation in each trace (left) and in total (right)	53
4.12 Delays in each period (Boxplot)	53

List of Tables

3.1 Patients information	32
4.1 Evaluation of algorithm results	44

Chapter 1

Introduction

1.1 Nervous System and EEG

The human brain is a complex organ which belongs to the nervous system, the most complicated human system. To understand and to explain the countless signals originated from the brain is used the electroencephalograph, which is a non-invasive instrument now used daily and capable of providing important information on the pathological state of the brain.

1.1.1 Nervous System Anatomy

The nervous system is a complex of organs responsible for receiving external and internal stimuli to the body and for processing coordinated voluntary and involuntary effector responses. It is also associated with multiplex psychic function, such as emotions, learning and memory. All organs that compose the system are made up of nervous tissue, whose fundamental unit is the neuron. It is classified anatomically in a peripheral part, which plays the role of transmitting signals to and from extra nervous organs (peripheral nervous system or PNS), and a central part (central nervous system or CNS), which is able to process the information that comes from PNS, providing responses that will be redistributed throughout the body [1].

The CNS consists of the encephalon, which is enclosed by the skull, and the spinal cord, which is instead located in the spinal canal. The encephalon in turn includes the brain, cerebellum and medulla oblongata. These three structures are covered by some membranes called meninges, which are divided into three layers:

- **Pia mater** - delicate and closest to the brain
- **Arachnoid mater** - middle of the meninges
- **Dura mater**- thick and near to the skull and vertebrae

There is also another protective barrier called blood-brain barrier (BBB) which is able to limit the solutes exchange between blood and brain. The BBB prevents the passage of many substances that circulate in the blood, such as toxic substances or metabolites, which could act as neurotransmitters and interfere with brain synaptic communication.

What allows the brain to function are neurons. There are approximately one thou-

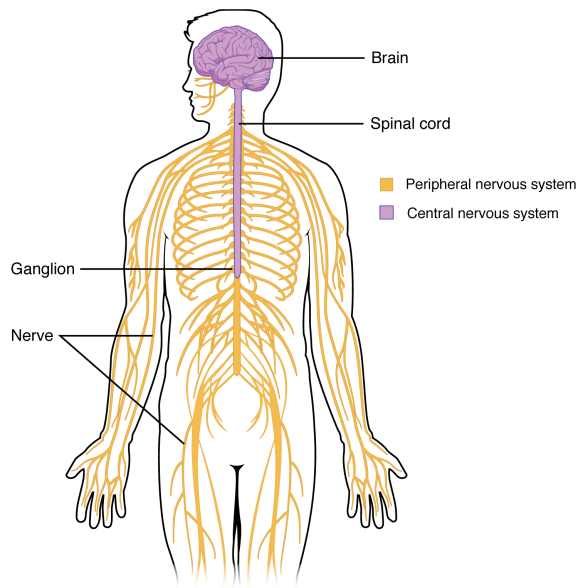


Figure 1.1: Central and Peripheral Nervous System

sand billion neurons in the brain, which are divided in a complex network. Neurons allow the propagation of the nerve impulse so that the brain is able to perform all its necessary for a good human body's health. Besides neurons, in even greater numbers, there are cells known as glia that have a supporting function into the brain [2].

1.1.2 Neurons

Neurons are the nervous system fundamental processing cells. They are hardwired for the electric signal generation and propagation along their membranes to other neurons or efferent cells. The main responsible for electromagnetic impulse propagation are the pyramidal neurons which are made up three parts (shown in figure 1.2): soma, axon and dendrites.

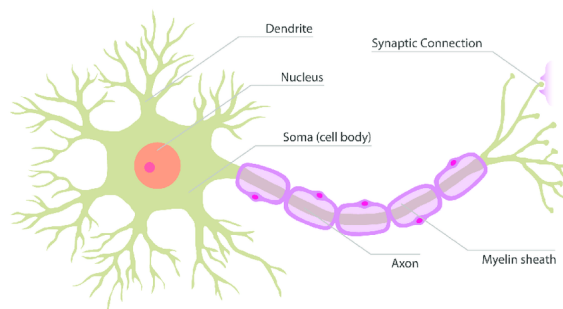


Figure 1.2: Structure of a neuron

In the soma, which is the central part of the neuron, the nucleus and other organelles responsible for the main cellular functions reside. Dendrites are the neuron's part that receives and transmits information to other neurons through junctions called synapses, which are small areas that allow chemical and electrical communication. The axon, on the other hand, has the task of transmitting the electrical signal to other nerve cells. The axon terminal part consists of a series of synaptic buttons

that allow communication between neurons and between the neuron and another cell. The soma has a simple plasma membrane, while the axon membrane can be coated with up to two layers of myelin, which is an insulating substance, consisting mainly of lipids and proteins. The myelin presence or absence makes axon myelinated or unmyelinated respectively. The myelin layers assemble oligodendrocytes and Schwann cells belong to the central nervous system and to the peripheral nervous system respectively and they are known as the myelin sheath.

The myelin sheath is not continuous, but every 1-3 mm has some interruptions called nodes of Ranvier. The myelin sheath alternation is necessary for impulses conduction (saltatory conduction); for this reason, action potentials can only be triggered in Ranvier nodes and they propagated jumping from one node to another. First of all, this type of conduction guarantees a speed conduction increase in the nerve impulses and secondly it allows energy saving because the depolarization occurs only in Ranvier's nodes.

According to the morphological point of view (depending on the neuritis structure), neurons are divided into:

- **Unipolar neurons:** they have only a neuritis that could work as axon or dendrite.
- **Bipolar neurons:** they have an axon and a dendrite that originated from two opposite cell body poles.
- **Multipolar neurons:** they have an axon and several dendrites that originated from different cell body points.
- **Pseudounipolar neurons:** they have a neuritis that originates in the soma end it splits into a T (one branch directed toward the periphery and one towards the CNS).

1.1.3 Nervous System Physiology

Neurons exploits complex signal propagation mechanisms. Even in rest condition, their membrane is endowed with a polarization known as membrane potential. The membrane potential is due to the ionic exchanges that occur between the membrane two sides (inside and outside the membrane) through the ion channels in the phospholipid bilayer. These channels do not allow passage to any ionic species, but are highly specific towards some ions such as sodium and potassium. This leads a charges of opposite sign difference on the two membrane sides. Moreover, channels can always be open and in this case they are responsible for the resting membrane potential (passive channels); on the contrary, there are channels whose opening is due to electrical, chemical and mechanical stimuli (active channels). Ions that generate charges difference are mainly Na^+ (sodium ion), K^+ (potassium ion) and Cl^- (chlorine ion).

During the resting condition, there is a high potassium concentration inside the cell, while outside there is a high sodium and chlorine concentration. Due to the different ion species concentration between inside and outside the cell, sodium tends to enter (because of concentration gradient), while potassium tends to exit, generating a electrical charges displacement and ,therefore, generating current. However, since

the membrane has a different permeability based on the ionic species (it is more permeable to potassium), potassium is able to exit the membrane more easily than sodium enters. This causes a charge imbalance which leads to a negative internal potential (-65 mV/-70 mV). To maintain the equilibrium concentration that leads to a negative potentials inside the cell, sodium-potassium pumps are necessary. They generate opposite species flows respect to the concentration gradient: potassium, therefore, will be pushed inside, while sodium will be pushed out. In this way, the total flux in the membrane will be equal to 0. However, in response to electrical stimulus, voltage-dependent channels come into operation: they are selective for sodium ions which are now able to enter inside the cell, depolarizing the membrane, i.e. increasing the membrane potential. For this reason, it is said that the neuron is an excitable cell: when it is crossed by a nerve stimulus, it modifies its ions balance so that the inside becomes positive and the outside becomes negative.

The action potential is initially triggered by a depolarization that have to exceed a threshold level, defined as the activation threshold, in order to allow the sodium voltage-channels opening, creating a net sodium ions flow into such to overcome the passive potassium migration toward the outside.

The action potential generation can be summarized in four steps [3]:

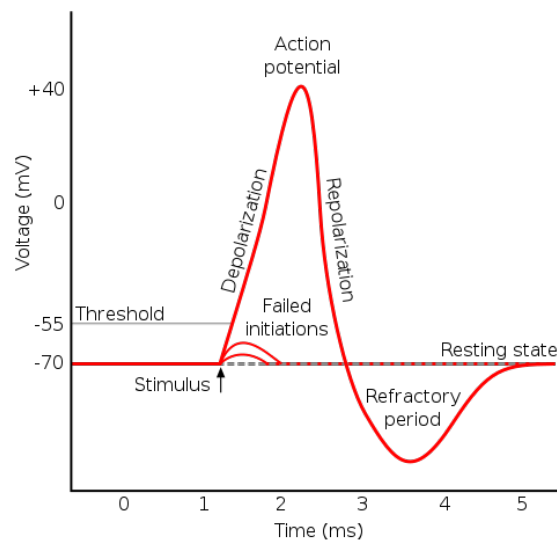


Figure 1.3: Action potential

1. **Depolarization:** from the rest state, once the threshold value is exceeded (about 55 mV), the potential increases until it approaches the sodium ion equilibrium potential value (+58 mV).
2. **Repolarization:** the membrane return to its initial condition after a short period because the sodium channels opening in temporary, indeed the membrane is again permeable predominantly to potassium.
3. **Hyperpolarisation:** the membrane permeability to potassium, during the repolarization phase, is higher so that a potential lower (more negative) than the rest condition potential is reached. The period in which the membrane potential is lower than the resting potential is called relative refractory period.

During this period, even if a new stimuli arrive that would cause the sodium channels reopening, the action potential does not trigger.

4. **Back to the resting state:** the membrane potential returns to its initial value because the potassium permeability value has re-established.

1.1.4 EEG Signal Characteristics

To investigate the cortical functions, the electroencephalographic signal (EEG) is studied. The EEG signal is the result of pyramidal neurons electrical activity, which are closest to the brain cortex. The neurons operation is poorly synchronized, except in particular pathological cases or induced cases. For this reason, the EEG signal will have a noisy appearance and therefore it is difficult to recognize typical waveforms; accordingly, the EEG is a random process that can only be describe in statistical terms. Until the 1970s it was the only way to investigate inside the skull. From to those years onwards, the development of CT scans and NMR has allowed us to have very precise anatomical brain images, leading to disuse of the EEG. A lot of diseases are due to anatomical brain alterations and these new medical instruments made it possible to identify abnormalities with a spatial resolution of 1 mm, while a source localization through the EEG signal could not have been so precise. However, CT scan and NMR have a poor temporal resolution while the EEG signal, from the point of view of localization over time, is unsurpassed. If an electrical change occurs in the scalp, this can be clearly read instantly in the EEG. In the 90s an attempt was made to combine the two information, that is a higher temporal resolution of the EEG with a better spatial resolution of the NMR and CT, however, leading to poor research results. Today, however, there are instruments on the market that perform both functions, but there are also analysis techniques such as functional magnetic resonance, which at the same time allow events to be located in a fairly precise way over time by combining an excellent spatial localization.

The two clinical applications in which the signal is irreplaceable are:

1. **study of epilepsies**
2. **brain-death observation**

In addition to these applications, electroencephalography has currently developed a high resolution acquisition system consisting of 512 electrodes that allows for better spatial localization. The EEG is also used for the evoked potentials studies, which are responses of the brain following external stimuli and they are used to diagnose diseases such as multiple sclerosis; it can be used also for sleep analysis because it is able to change its characteristics according to the level of sleep. The EEG signal can be affected by many artifacts and it is therefore important to be able to distinguish whether a variation in the graph may be due to the activity of neurons or to an artifact. For example, motion artifacts are visible in the graph, but to better understand where they are in the signal, videoelectroencephalography was introduced, which precisely captures the subject while an EEG is taken.

The EEG amplitude varies from a few μV to a few hundreds of μV , divided into three bands: low ($< 30\mu\text{V}$), medium ($30-70\mu\text{V}$) and high ($> 70\mu\text{V}$). Regarding morphology, it can be polymorphic or monomorphic. Polymorphic when it has

potentials belonging to the same frequency band but with different amplitude and irregular periodicity. Monomorph instead when it has a succession of potentials, as well as of the same frequency band, also of the same amplitude. If the signal is present in both hemispheres (right and left), it is said to be symmetrical (there are events that occur only in one hemisphere: asymmetric events). If events occur simultaneously in the two hemispheres, they are said to be synchronous, otherwise asynchronous.

Although the signal is difficult to analyze from a morphological point of view, a frequency band can be identified that contains most of the information. Regarding basal EEG, i.e. taken on the scalp surface, the frequency band is between 0.1 and 80 Hz. Actually, up to 20 years ago the band was up to 40 Hz, but then we saw that there is information also on higher frequencies, even if from a clinical point of view it is not known what they represent.

The signal band is then divided into sub-bands:

- **Beta activity** - β waves occupy the frequency band between 12 to 30Hz and they are divided into β_1 (12-20Hz) β_2 (20-30Hz). They are predominant in a subject with open eyes engaged in any brain activity, but also in sleep during REM or during some drugs intake.
- **Alpha activity** - α waves occupy the frequency band between 8 to 12Hz. They occur mainly in an awake subject with closed eyes. They are present in both hemispheres and the absence in one of two indicates a pathological state.
- **Theta activity** - θ waves have frequency in the range 4-8Hz. They are dominant in newborn, while the in the adult the may indicate brain diseases. They also occur in states of emotional tension, hypnosis and in a state of semi-sleep within minutes of falling asleep.
- **Delta activity** - δ waves have frequency less than 4Hz. They are the characteristic waves of sleep; they are not present in the adult waking state although they are predominant in childhood.

Typical rhythm patterns are shown in figure [1.4](#)

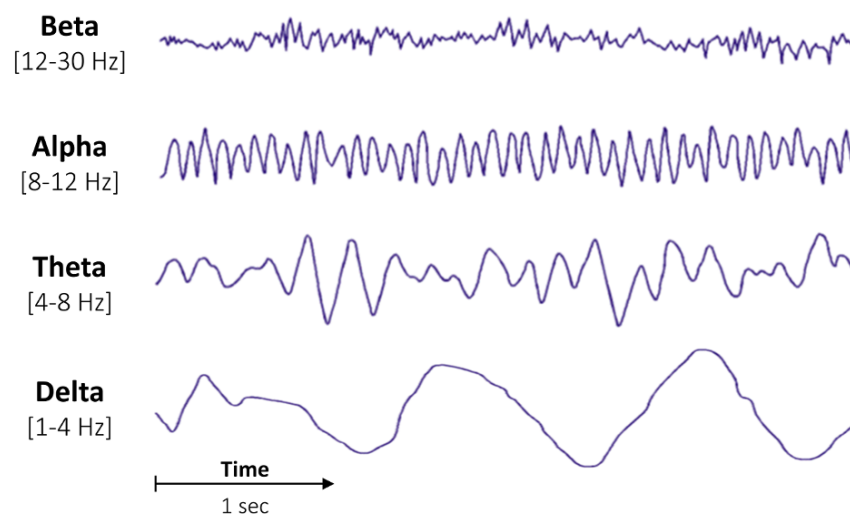


Figure 1.4: Brain wave patterns

1.1.5 The International 10-20 System

Since different brain areas are specialized in different functions it is important to take the EEG signal from the whole scalp. It is also necessary that the picking up is always the same by whoever makes it and in any place. For this reason, a series of rules for electrode placement has been devised. The 10-20 standard is the standard for electrode placement in EEG, shared throughout the world. Four reference points are taken for the skull. The nasion is the fossa above the root's nose. The inion is the landmark located posteriorly along the mid line of the skull where there is a slight protuberance of the bone. Finally, there are two preauricular points which are located below and in front of the auricle on either side of the head. Electrode names correspond to the brain areas in which they are placed. In particular:

- Fp: frontopolar
- F: frontal
- C: central
- T: temporal
- P: parietal
- O: occipital
- Z: medial line

You have to think about drawing an imaginary line. First, the length of the curve that passes over the scalp and medially connects the nasion and inion is measured with a tape. 10% of this distance is calculated and starting from the nasion and moving each time by 10%, we arrive at a point where we can mark a parallel to the skull. Along this parallel there are the electrodes FP₁ and FP₂, which lie above the orbits. The electrodes found in the left hemisphere have odd subscripts, those found in the right hemisphere have even subscripts.

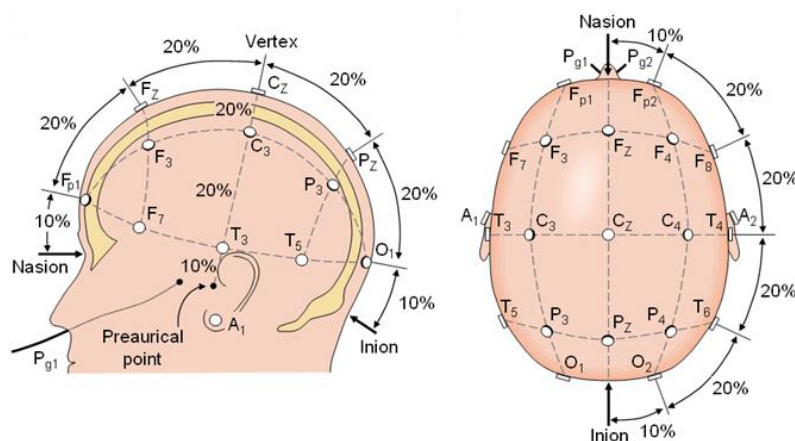


Figure 1.5: International 10-20 system

To know how far the frontopolar is from the nasion, on the parallel the nasion-inion distance is measured laterally passing over the preauricular point and 10% is calculated. If you move medially from the nasion by 10%-20% (along the skull mid line), there is an electrode FP_z (it has a subscript z because it is neither on the right nor

on the left, but in the center of the skull). If from FP_z we move toward the left on a line that goes from FP_1 to O_1 medially we find F_3 ; if you go down to the line that connects FP_1 and O_1 , laterally we find F_7 . On the other side there are F_4 and F_8 . O_1 and O_2 are the rear points to FP_1 and FP_2 . In the skull center, C_z is located. Extending to the left there are C_3 (between FP_1 and medial O_1) and T_3 (between FP_1 and lateral O_1); the same applies to the right. The rear electrodes are P_z , P_3 and P_4 .

In total there are 19 electrodes. The 10-20 standard does not prescribe a number of electrodes, but prescribe their positions. The full 10-20 standard is when you move in 10% steps: in this case new electrode lines appear and you get up to 73 electrodes. The electrodes just described are all expolarants electrodes. To pick up a signal, a reference is required. The most used references are placed on the earlobe and are indicated with the positions A_1 and A_2 . The left electrodes can refer to A_1 and the right ones to A_2 , or they can all refer to one of the two or to their average. In addition to the lobes, other references such as an electrode placed on the mastoid bone or on the chin can be used. In some cases it is preferred to use a non-cephalic reference, such as the mean of the potentials.

1.2 Epilepsy

Epilepsy is a CNS system pathology caused by cerebral cortex neurons malfunction. It is a clinical condition due to a sudden onset of neurons hyper-synchronize. Depending on the area of the cerebral cortex that is affected, the symptoms can vary; they are alteration in the state of consciousness, behavioral alterations and motor and sensory function alterations, but the most common symptoms are seizures. The physiological mechanism that leads to the epileptic crisis is an imbalance between inhibitory and excitatory action, which leads to a transmembrane ionic exchanges alteration, resulting in a neurons hyper-excitability. About 1% of the world's population suffers from epilepsy and nearly 80% of cases are found in developing countries. In 2013, epilepsy caused 116.000 deaths, up from 111.000 in 1990.

Epilepsy becomes more common in elderly people, even if it has a high prevalence even in the first year of life, so the diagnosis immediately after birth is important. The mortality rate in epilepsy patients is 2-3 times higher to that of the general population and it's higher in males. Death can only be related to epilepsy (suicides, tumors, ischemic heart disease) or it can happen accidentally during a crisis.

Epileptic seizures can be divided into four phases. The phase preceding the epileptic seizure is called *pre-ictal*. During this phase, there are sensory alteration in the patient. Then follows the *ictal* phase which is the phase of the actual seizure in which neurological symptoms such as spasms and loss of consciousness occur. Afterward, *post-ictal* phase leads the subject to a restoration of the normal condition. Finally, between two seizures, there is the *inter-ictal* phase.

1.2.1 Classification

There are several classifications of epilepsy, but despite this, all the classifications are distinguished in focal (or partial) seizures and generalized seizures. The first type of seizure concerns neurons (which participate in the discharge) which are present only in one region of the cerebral cortex; the second concerns neurons present throughout the cortex.

According to ILAE (International League Against Epilepsy) [4], in 1989 epilepsy was classified according to its cause (etiological approach). In particular, it is distinguished in idiopathic epilepsies, to which it does not recognize precise and identifiable causes but is thought to be of genetic origin; symptomatic epilepsies, which depend on the nervous system structure alterations (such as brain tumor) and finally cryptogenic epilepsies, the origin of which is unknown. In 1981, ILAE classified epilepsy based on clinical and EEG features [5]. They are divided into:

- **Simple partial seizures:** in this type of seizure the patient does not lose consciousness and is able to tell what happened. Since only some of the brain areas are affected, depending on the area, spasms may occur only in some fingers, in one arm or in the whole body. There may also be sensory phenomena such as heat or cold sensations, loss of taste, loss of vision, dizziness or sensation of free-falling. Psychic symptoms such as memory loss, loss of reality and hallucinatory fits, emotional crises and difficulty speaking may also occur.
- **Complex partial seizures:** the patient loses consciousness. The loss of consciousness may not be complete, in the sense that the patient can understand what is happening nearby. There is an aura. It is characterized by the patient activity arrest, who often has a fixed gaze and manifests oral, gestural, mimic and ambulatory automatism. After the seizure, a period of confusion is followed by a slow recovery of normal activity.
- **Generalized seizures:** discharges begin simultaneously from both brain hemispheres. They are characterized by loss of consciousness and the absence of aura and they can come unexpectedly without any particular antecedent symptoms. Generalized seizures are divided into:
 - **Primary generalized tonic-clonic seizure (GTCS):** it is the most common generalized epilepsy. It begins with a tonic phase in which the body stiffens, the patient loses consciousness and falls. Then follow a clonic phase which can last several minutes and which involves violent agitation of the whole body.
 - **Absence seizures:** They last a few seconds and they are more common in children. Absence seizures are characterized by the state of consciousness suspension in which the subject remains with his gaze lost in the void. At the end of the seizure, the patient does not remember anything. This type of epilepsy is characterized by abnormalities in the EEG trace in which spike and waves can be detected.
 - **Myoclonic seizures:** they consist of short and sudden muscle contractions in different parts of the body.

- **Clonic seizures:** they are repeated in the same muscle groups regularly and they consist of a bilateral tremors series that occur to the trunk and limbs.
- **Tonic seizures:** they present only the tonic phase of muscle stiffening followed by a sudden loss of consciousness.
- **Atonic seizures (astatic seizures):** these kind of seizures cause a total suspension of the localized or generalized muscle tone that leads the patient to fall on the ground.

1.2.2 EEG Waveform Abnormalities

First of all, it should be noted that not all those who report an EEG use the same terms or give them a similar meaning. The glossary of the IFCN (International Federation of Clinical Neurophysiology), which often derives from compromise choices between the various positions, is the one that is universally accepted; it also focuses attention on the morphological characteristics of the graph elements and does not become unbalanced in terms of clinical interpretation.

A distinction must be made between *paroxysm* and *seizure pattern* or *discharge* [6]. The first is a single graph element, which begins and ends abruptly, which is clearly distinguished from the background activity. The second means a phenomenon lasting a few seconds or more, consisting of repeated epileptic graph elements, with a fairly well recognizable beginning and end. Epileptiform graph elements are described below.

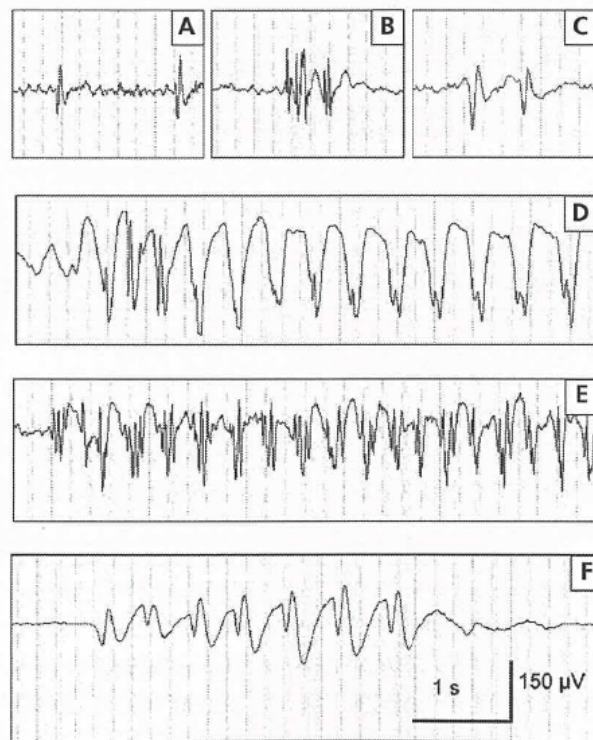


Figure 1.6: EEG waveform abnormalities

- **(A) Spike:** transient graph element, clearly distinct from the background activity, with a negative main component, mono-bi-triphasic, variable amplitude ($50 - 100\mu\text{V}$) and very short duration ($20 - 70\text{ms}$).
- **(B) Polyspike complex:** sequence of two or more spikes.
- **(C) Sharp wave:** transient graph element, clearly distinct from the background activity, bi-triphasic, variable amplitude ($100 - 200\mu\text{V}$) and a duration of $70 - 200\text{ms}$.
- **(D) Spike and slow wave complex:** paroxysm characterized by a spike followed by a slow wave: it can have a frequency of 3 Hz (typical) or less (atypical).
- **(E) Polyspikes and slow wave complex:** polyspikes followed by a slow wave.
- **(F) Sharp and slow wave complex:** sharp wave followed by a slow wave.

1.2.3 Spike and Wave

Particular attention deserves the spike and the wave. It is a visible pattern in different types of epilepsy, but it is most noticeable during absence seizures. It is caused by a bilateral synchronous firing of neurons that go from the neocortex to the thalamus. The reason for the genre of spike and wave is still being studied. One hypothesis is that the spike is generated by the neuronal membrane potential, also called Paroxysmal depolarizing shift which was thought that it was generated by a large EPSP (post synaptic excitatory potential) due to a lack of synaptic inhibition, which allowed the triggering of voltage gated sodium channels which in turn generate a current that gives rise to the action potential. Calcium channels are also activated but have a less marked effect than sodium channels. The calcium channels, however, leading to an increase in the concentration of intracellular calcium, in turn lead to the activation of the potassium channels which, instead, lead the membrane to repolarization with consequent hyperpolarization. The long phase of depolarization, which causes an action potential train, constitutes the spike, while the subsequent phases of repolarization and hyperpolarization determine the wave [7].

However, other studies [8] have shown that synaptic inhibitory activity remains present during paroxysmal depolarizing shifts for which the hypothesis that the spike and wave is caused by a large excitatory postsynaptic potential and by the almost absence of inhibitory postsynaptic potentials (IPSPs) is not accepted. Indeed, due to the activation of the postsynaptic GABA receptor, there is an increase in the concentration of intracellular chloride which leads to a post-synaptic inhibitory potential. Especially during seizures, when depolarization occurs, there is a significant activation of the GABA receptors which leads to a large concentration of intracellular chloride as long as the inhibitory current due to GABA exceeds the reversal potential and the chlorine ions leave the cell, leading to a reduced or inverted amplitude of IPSPs. Other receptors that have been shown to play an important role in the generation of spike and waves are the metabotropic glutamate receptors, in particular mGlu4. Some studies [9] have shown how the elimination of mGlu4 receptors from mice allowed them to resist induced absence epileptic seizures, precisely because the missing receptors did not allow the release of glutamate and GABA into the thalamocortical network. Therefore, an increase in mGlu4 activity is associated with spike and wave discharges during absence seizures, so much so that currently drugs capable of blocking these receptors are also used to treat absence epilepsy.

1.2.4 Diagnosis and Therapy

The diagnosis of epilepsy is made first of all through a clinical investigation that allows to have a clear description of the episodes that the doctor will evaluate if they are attributable to the disease [10]. In this case, instrumental examinations are performed. The first is the electroencephalogram which is able to identify any anomalies of epileptic origin that could confirm the diagnosis, but a possible absence could not exclude it. Imaging techniques such as magnetic resonance and computed tomography allow us to study any structural alteration (such as any brain tumors) that may be the cause of epilepsy. Also radio tracer tests such as PET and SPECT can highlight the presence of areas functionally hyperactive or hypoactive. Blood

tests can be used to identify metabolic alterations or genetic diseases that may be associated with seizures. Instead, neuropsychological tests allow you to assess patients' thinking, memory and language skills, helping to identify the affected brain areas.

Epilepsy is mainly treated with antiepileptic drugs which are usually prescribed after the second seizures. The drug choice is based on the type of epilepsy that the subject presents and generally, at least initially, includes only one drug. The effectiveness of the therapies is evaluated over weeks or months and in any case taking into account the frequency of epileptic seizures. In cases where patients suffer from drug-resistant epilepsies and in which it is possible to trace a stable and unique origin and whose removal does not cause further neurological problems, it is possible to use surgical therapy. Surgical therapy can be of the resective type, i.e. the epileptogenic area is completely eliminated; or it can be palliative, meaning that it is used to reduce the seizures frequency and severity.

Chapter 2

Mathematical Concepts

To understand the following discussion, it is advisable to introduce some mathematical concepts. In particular, methods for eliminating EOG and EMG artifacts and main technique that exploits the algorithm to search for spike and wave in the eeg signal will be described.

2.1 Blind Source Separation (BSS)

The blind source separation algorithms have made it possible to overcome the limits of classical methodologies and obtain more effective denoising. The BBS algorithms principle is to succeed in separating a signal that is composed of other signals. The problem can be thought of as if it were composed of three elements: the sources, which generate the signal, the communication channels which weigh the source signals and the sensors. A simple example would be when you search for oil underground by detonating explosive charges. In this case the communication channel is the soil and what is measured are the return echoes. A mixture is measured which is the sum of all the echoes arrived and the algorithm wants to separate the mixture into the single echoes. Another example is the cocktail party problem where many speakers talking at the same time in the same room and some microphones pick up the sound, on which the BBS algorithm can be applied to separate the sources. There are several mathematical models that are able to describe the method, but the simplest is the instantaneous linear model [11] [12].

It is supposed to have n different sources picked up by m sensors, with $m \geq n$. The mathematical model can be described by the following equation:

$$\mathbf{x}(t) = \begin{bmatrix} x_1(t) \\ \vdots \\ x_m(t) \end{bmatrix} = \begin{bmatrix} a_{11} & \dots & a_{1n} \\ \vdots & \ddots & \vdots \\ a_{m1} & \dots & a_{mn} \end{bmatrix} \begin{bmatrix} s_1(t) \\ \vdots \\ s_n(t) \end{bmatrix} = \mathbf{A}\mathbf{s}(t) \quad (2.1)$$

where t are the time samples of the m signals, $x(t)$ is a matrix of size equal to $m \times t$, $s(t)$ is a matrix of size equal to $n \times t$ which contains samples of the n sources signals; finally A is a matrix ($m \times n$) called mixing matrix. Assuming that the observed signals have zero mean, each row of $x(t)$ contains the m -th signal recorded by the

sensor, as well as each row of $s(t)$ contains the n -th source signal. To reconstruct the $s(t)$ matrix containing the sources signals, three steps are necessary:

1. Estimate the mixing matrix A , whose product for $s(t)$ gives $x(t)$
2. Invert the mixing matrix A
3. Apply the inverse A^{-1} to the observed signals, in order to obtain the sources:

$$s(t) = A^{-1}x(t) \quad (2.2)$$

In this case the simple inverse matrix A^{-1} is used due to, as for EEG, the number of sources is equal to the number of available channels. On the other, if the number of channels had been greater than the number of sources, the pseudoinverse matrix should have been calculated, as explained in [12].

To solve the problem, it is necessary to impose conditions on the mixing matrix A or in the sources $s(t)$. Generally, BSS algorithms impose conventions on the latter and they take a different name according to the conditions given.

2.1.1 Second Order Blind Source Separation

To estimate the mixing matrix, there are methods that exploit second order statistical moments. In particular, these methods pose the condition of non-correlation of the sources. One of the algorithms, used in this study to remove EOG artifacts, is the SOBI algorithm, which assumes the temporal non-correlation of the sources [13]. The algorithm can be briefly described in two steps [11]: data whitening and rotation matrix creation. In the first step, a whitening matrix W is used, such that, applied to [2.1], it is obtained:

$$WAA^TW^T = I \quad (2.3)$$

where I is an identity matrix. By multiplying the observed signals $x(t)$ by the matrix W , their whitening is obtained, indicated by:

$$z(t) = Wx(t) = Us(t) \quad (2.4)$$

where $U = WA$. We can write the covariance matrix of $x(t)$ as:

$$\hat{R}_{xx} = \frac{1}{T} \sum_{t=1}^T x(t)x(t)^T \quad (2.5)$$

which can be factored as:

$$\hat{R}_{xx} \approx A\hat{R}_{ss}A^T \quad (2.6)$$

where \hat{R}_{ss} is the covariance matrix of $s(t)$. \hat{R}_{ss} is a diagonal matrix with the variance values of the sources on the diagonal. Given the equations [2.4] and [2.6], we note that the matrix W is the matrix that diagonalizes \hat{R}_{xx} and is therefore determinable through the eigenvalues and eigenvectors of the matrix \hat{R}_{xx} .

The second step consists in the evaluation of a rotation matrix U such that: $U = WA$. The mixing matrix A can be obtained by:

$$A = W^{\#}U \quad (2.7)$$

The U matrix is a unity matrix which can be considered a rotation matrix calculable through a common diagonalization between correlation matrices of the whitening observations $z(t)$ at different delay values τ :

$$\hat{R}_{zz} = \frac{1}{T} \sum_{t=1}^T z(t)z(t + \tau)^T \quad (2.8)$$

which can be factored as:

$$\hat{R}_{zz}(\tau) \approx U\hat{R}_{ss}(\tau)U^T \quad (2.9)$$

Having found U and W , we can calculate A as in [2.7](#), so it is now simple to estimate the sources as [2.2](#).

2.1.2 Canonical Correlation Analysis

The canonical correlation analysis (CCA) as BSS technique, is used for muscle artifact removal. Considering [2.1](#) and assuming that the mixing matrix is linear, the goal is to estimate $W = A^{-1}$, forcing the sources to be mutually uncorrelated and maximally autocorrelated and $s(t)$ a square matrix [14](#). Since $W = A^{-1}$, the equation [2.2](#) becomes $s(t) = Wx(t)$. A signal $y(t)$ is created, which corresponds to the original signal $x(t)$ delayed in time, with a delay equal to 1:

$$y(t) = x(t - 1) \quad (2.10)$$

BSS-CCA algorithm, by removing the mean of each $x(t)$ and $y(t)$ row, is able to obtain two basis vectors, so that correlation between their projections is mutually maximized. Considering a linear combination of the $x(t)$ and $y(t)$ components:

$$\mathbf{u} = w_x^T x = w_{x1}x_1 + w_{x2}x_2 + \dots + w_{xm}x_m \quad (2.11)$$

$$\mathbf{v} = w_y^T y = w_{y1}y_1 + w_{y2}y_2 + \dots + w_{ym}y_m \quad (2.12)$$

where m are the observations and w_x and w_y are the weight vector which maximize the correlation ρ between \mathbf{u} and \mathbf{v} :

$$\begin{aligned} \max_{w_x, w_y} \rho(\mathbf{u}, \mathbf{v}) &= \frac{E[uv]}{\sqrt{E[u^2]E[v^2]}} \\ &= \frac{E[(w_x^T x)(w_y^T y)]}{\sqrt{E[(w_x^T x)(w_x^T x)]E[(w_y^T y)(w_y^T y)]}} \\ &= \frac{w_x^T C_{xy} w_y}{\sqrt{(w_x^T C_{xx} w_x)(w_y^T C_{yy} w_y)}} \end{aligned} \quad (2.13)$$

C_{xx} and C_{yy} are the autocovariance matrices of $x(t)$ and $y(t)$, while C_{xy} is their crosscovariance matrix.

To find the maximum correlation, it is necessary to carry out the first derivative with respect to weights w_x and w_y , in order to obtain:

$$\begin{cases} C_{xx}^{-1} C_{xy} C_{yy}^{-1} C_{yx} \hat{w}_x = \rho^2 \hat{w}_x \\ C_{yy}^{-1} C_{yx} C_{xx}^{-1} C_{xy} \hat{w}_y = \rho^2 \hat{w}_y \end{cases} \quad (2.14)$$

The problem is reduced to a eigenvalues and eigenvectors problem, where the correlation coefficient ρ is the square root of the eigenvalue, while the weights w_x and w_y are the eigenvectors.

Since $y(t)$ is $x(t)$ lagged by 1, they represent same data, so w_x and w_y also be almost similar and the equation [2.14](#) can be solved only for \hat{w}_x or \hat{w}_y . Trough this method, for each element of $x(t)$, we obtain the time course of the first pair of vectors u_1 and v_1 , where u_1 is the maximized autocorrelation:

$$v_1(t) = w_y^T y(t) = w_x^T x(t - 1) = u_1(t - 1) \quad (2.15)$$

Considering new pairs of weights vectors w_x and w_y , new vectors u_i are evaluated, using [2.14](#) and imposing the condition that new u_i are uncorrelated from the previous calculated. Therefore all the vectors u_i will be generated by linear combination of $x(t)$ which guarantee the maximum autocorrelation and at the same time their uncorrelation.

BSS-CCA algorithm is used for the separation of brain and muscle activity because of the relatively low autocorrelation value of artifactual components compared to neural ones, since the algorithm finds sources that are mutually uncorrelated and maximally autocorrelated sorted in descending order with respect to ρ .

2.2 Matched Filtering

For detecting the presence of a known signal within an unknown signal, it is possible to use the matched filtering technique [15](#). In particular, matched filter identifies a piece of signal that, although it may be covered with noise, is similar to the prototype signal to be identified. This occurs by correlating the known signal with the unknown signal, that is making the convolution between the unknown signal and the time reversed prototype signal. The technique goal is to maximize the signal to noise ratio when the signal is corrupted by stochastic noise. A typical example is the radar technology, where you want to evaluate the distance to an object by transmitting a signal on it and measuring how long it takes to return to the source. Therefore, to understand if the return signal is the one transmitted, it is necessary to correlate the received signal with a matched filter.

For example, if you send a sinusoid with a certain frequency, you can assume that the return signal is also a sinusoid that can be attenuated and delayed and mixed with noise. By applying the match filter to the return signal, if a performance threshold is exceeded, it can be said that the received signal is actually the transmitted one.

Considering [2.1](#), the signal is $s(t)$, the white noise that is added to it is $n(t)$, the filter which is the time reversed of the input signal and which maximize the signal to noise ratio (SNR) is $h(t)$, finally the output signal is $y(t)$. The match filter goal is to maximize the signal to noise ratio; it is a quasi-optimum linear filter. The peculiarity, is that despite it is a filter, it does not act on specific frequency bands, but it recognizes particular waveforms over time, which can be covered by noise; in fact the filter is able to increase the signal to noise ratio by reducing the noise band to that of the prototype [16](#) [17](#).



Figure 2.1: Basic filter structure

SNR is given by:

$$SNR(T) = \frac{\left| \int_0^T h(\tau) y(T - \tau) d\tau \right|^2}{\sigma^2 \int_0^T |h(\tau)|^2 d\tau} \quad (2.16)$$

where σ^2 is the noise variance. To obtain the matched filter signal $y_{MF}(t)$ is necessary to filter (i.e. convolve) the output signal $y(t)$ with the time reversed filter $h(-t)$:

$$y_{MF}(t) = y(t) * h(-t) = \int_{-\infty}^{\infty} y(t) h(t - T) dt \quad (2.17)$$

This method is equivalent to a normalized cross-correlation between the observed signal and the prototype. Assuming a white noise, the optimal filter that maximize [2.16](#) is $y(-t)$ (time reversed output signal). The optimal filter assumption is valid only for a white noise, so it is an ideality. In reality, the filter is only quasi-optimal because of the noise is not white.

2.2.1 Wavelet Example

An example is a wavelet included in a noisy signal [\[15\]](#). In this case the signal to noise ratio is given by the ratio between the wavelet peak amplitude and the noise standard deviation. Taking into consideration the wavelet in the figure: [2.2](#)

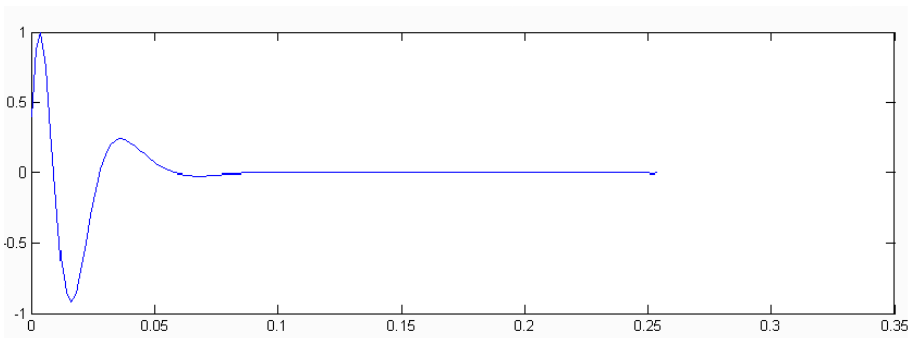


Figure 2.2: First 100 ms of wavelet

Wavelets were added to ten signals in [2.3](#) in order to obtain signals that vary their SNR from 0.2 to 2 from bottom to top.

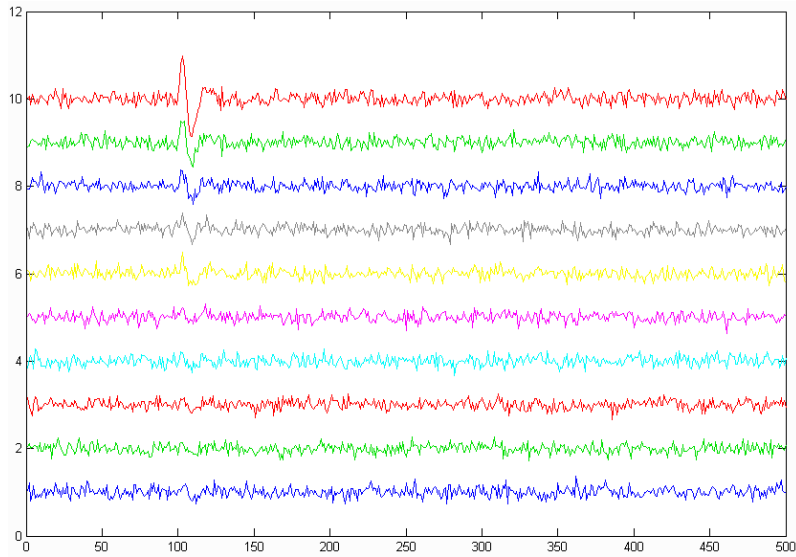


Figure 2.3: Noisy signals and wavelets

Making the crosscorrelation between the wavelet in [2.2](#) and the ten signals in [2.3](#), the matched filters in [2.4](#) are obtained. There is an improvement of the signal to noise ratio in each of the ten trace. You notice that the wavelet energy is maintained and its shape has been changed to zero phase because of in wavelet the crosscorrelation becomes auto correlation.

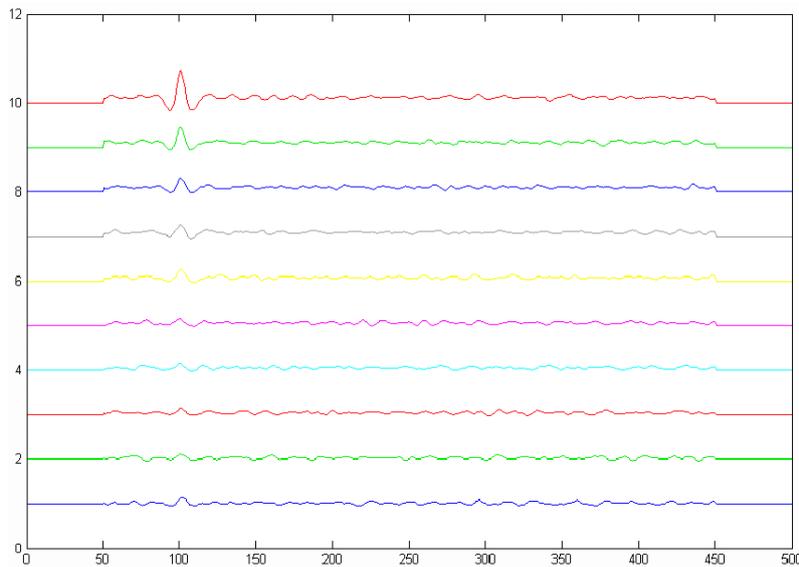


Figure 2.4: Matched filters results

Chapter 3

Materials and Methods

3.1 Dataset

A dataset made up of ten patients from the Cuneo hospital was used in this study. In particular the dataset is composed by epileptic patients in observation for some tens of minutes, in which seizures were introduced by light stimulation or hyperventilation. In [3.1](#), the electrodes used are highlighted, while patient information are listed in table [3.1](#).

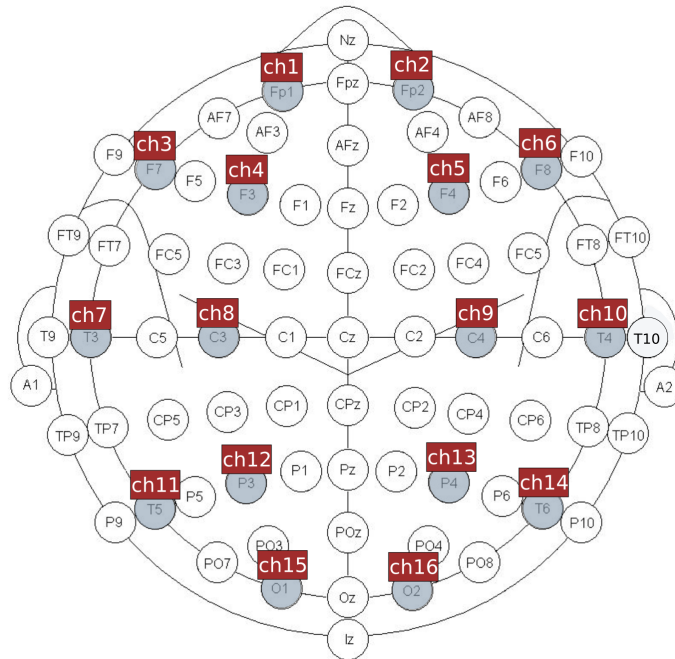


Figure 3.1: EEG channels distribution

The patients are all affected by generalized epilepsy, that means, as we learn in [1.2.1](#), they have seizures in both hemispheres. The montage used is a bipolar montage in which each electrode represents the difference between two adjacent electrodes, in particular channels used in the acquisition are the following: 'Fp2-F4', 'F4-C4', 'C4-P4', 'P4-O2', 'Fp1-F3', 'F3-C3', 'C3-P3', 'P3-O1', 'Fp2-F8', 'F8-T4', 'T4-T6',

Patient	Sex	Montage	Seizures	Origin	EEG Duration (min)
1	female	bipolar	8	generalized	13.76
2	female	bipolar	4	generalized	18.18
3	female	bipolar	1	generalized	21.35
4	female	bipolar	4	generalized	20.15
5	female	bipolar	1	generalized	20.08
6	female	bipolar	2	generalized	26.33
7	female	bipolar	11	generalized	36.86
8	male	bipolar	5	generalized	27.35
9	female	bipolar	3	generalized	21.13
10	male	bipolar	0	generalized	20.15

Table 3.1: Patients information

'T6-O2', 'Fp1-F7', 'F7-T3', 'T3-T5', 'Fz-Cz', 'Cz-Pz'.

3.2 Preprocessing

All signals were sampled with a sampling frequency of 128 Hz. A band pass filter, obtained as a cascade of a high pass filter with a low pass filter, was then applied. In particular, two IIR Chebyshev Type II filters were used, of order 5 and 6 respectively. The high pass filter has a cut-off frequency of 1 Hz, with attenuation of 20 dB in the stopband at 0.75 Hz. Instead, the low passfilter has a cut-off frequency of 40 Hz, with attenuation of 20 dB in the stopband at 44 Hz.

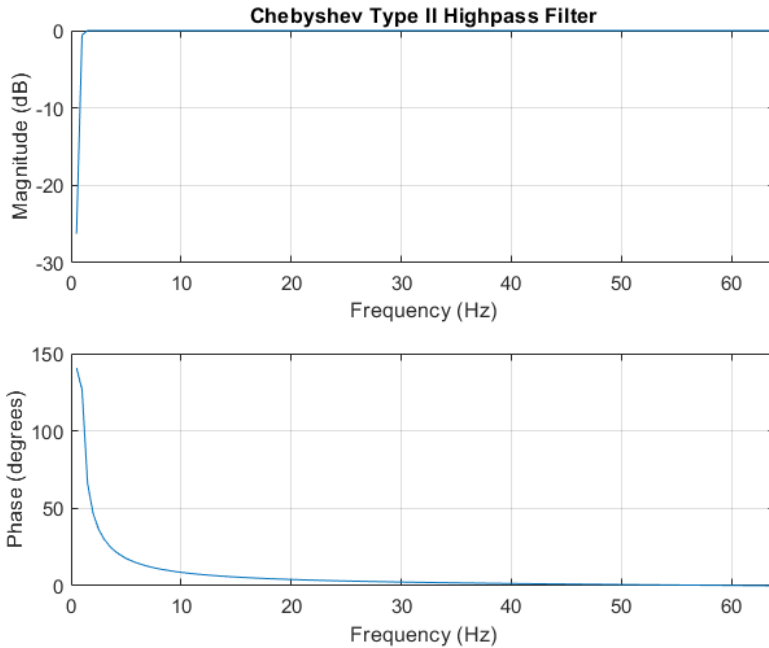


Figure 3.2: Bode diagram Chebyshev type II highpass filter, order 5

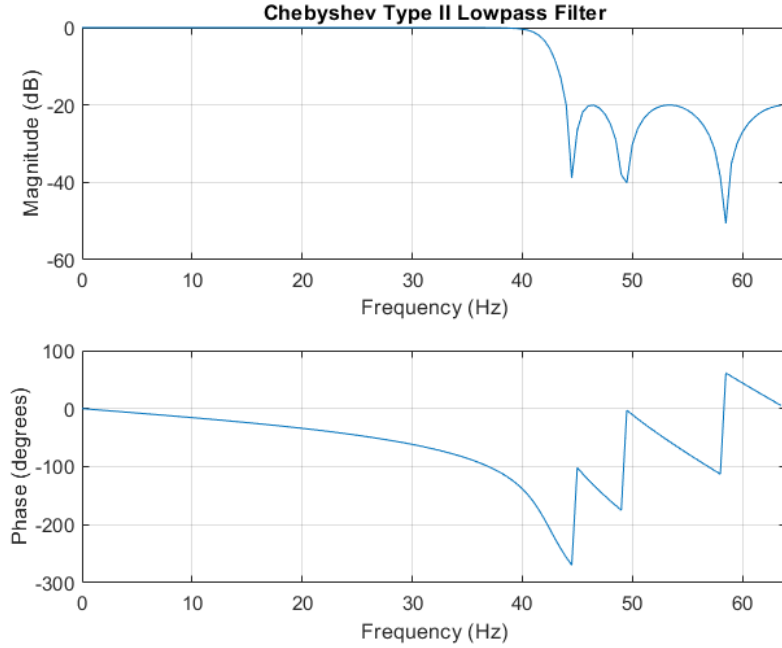


Figure 3.3: Bode diagram Chebyshev type II lowpass filter, order 6

3.2.1 EOG Removal

An automatic tool by German Gomez-Herrero et al. [18] [19] was used to remove the EOG artifacts. In particular, Gomez uses the SOBI algorithm described in [2.1.1]. The mixing matrix A is estimated considering the uncorrelated sources as explained in [2.1.1] and going to evaluate the matrix that better diagonalize a set of observation covariance matrices at different delay values.

To identify the sources that give rise to the artifact, a measure of the complexity of the signal based on the fractal dimension was used. The frequency spectrum of the ocular activity sources is concentrated more on low frequencies, while the spectrum of the EEG signal is more distributed. For this reason, the fractal dimension of the EEG spectrum turns out to be greater than that of the ocular activity, so it is easy to recognize them. Finally, having the mixing matrix A and the artifact sources, the EEG signal (clean) $\hat{x}(t)$ can be reconstructed by multiplying the signal itself with the mixing submatrix A_{EEG} which contains only the neural sources (no artifacts) and its pseudoinverse matrix $A_{EEG}^\#$ [19]:

$$\hat{x}(t) = A_{EEG}^\# A_{EEG} x(t) \quad (3.1)$$

The algorithm was applied on signal epochs of 200 s. For artifacts such as EOG, which has regular rhythms, it is advisable to use long windows, but it is important not to exceed as too long a length could cause the removal of non-artifactual neural sources. Below, two images relating to the same signal epoch before and after EOG removal are shown.

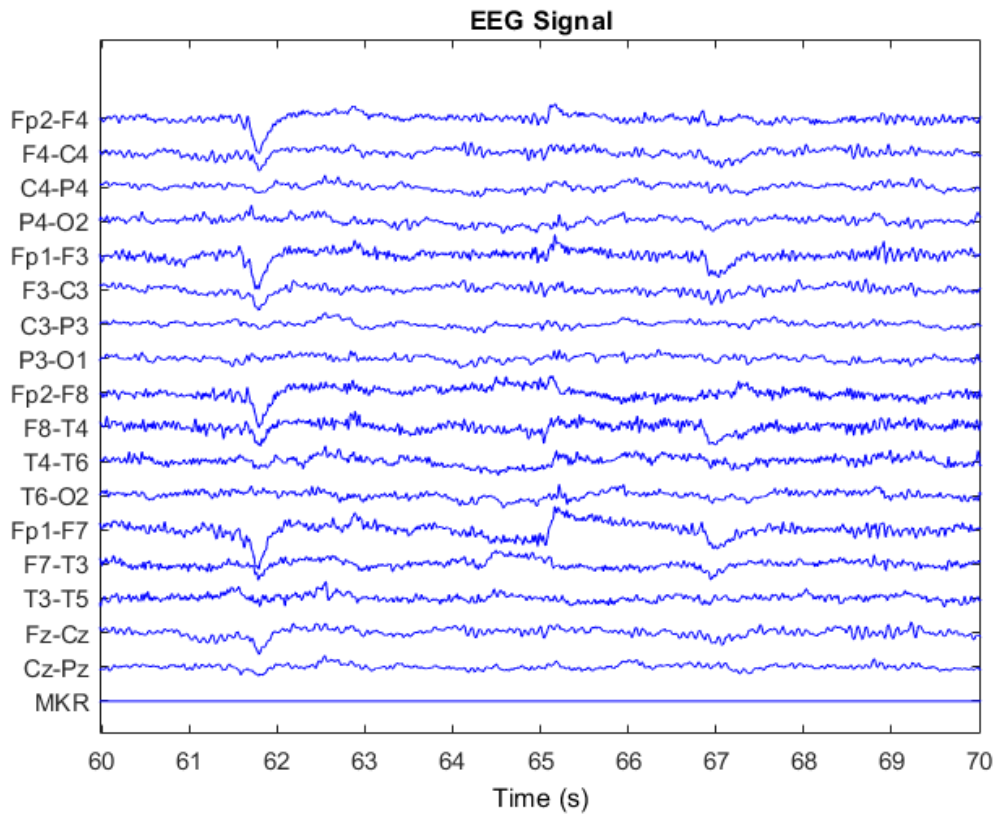


Figure 3.4: 10 seconds of EEG signal after bandpass filter and before EOG removal

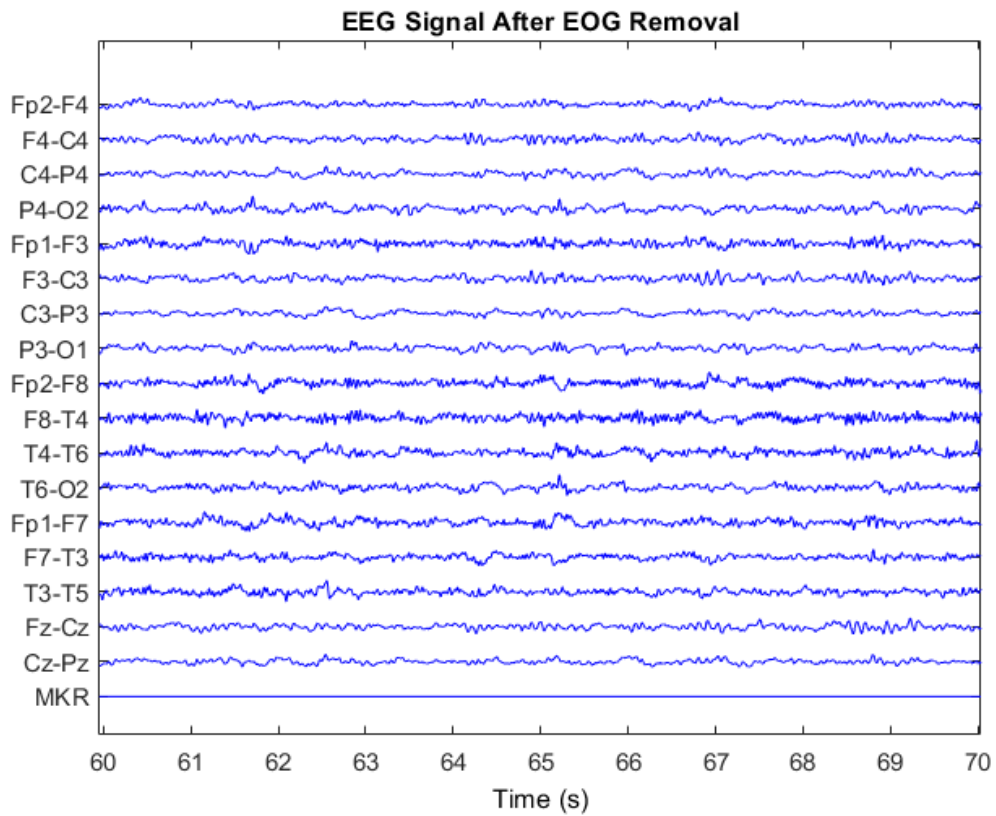


Figure 3.5: 10 seconds of EEG signal after EOG removal

3.2.2 EMG Removal

The method of German Gomez-Herrero et al. [18], which uses the BSS-CCA algorithm in 2.1.2 was also used to remove the EMG artifact. The mixing matrix A is estimated assuming the sources are mutually uncorrelated but maximally autocorrelated. Indeed, according to [14], the autocorrelation value of the EMG components is much lower than the neural components and therefore it is easy to separate them. The criterion used in [18] for the identification of the artifactual components is based on the fact that most of the electrical activity of the EMG signal is higher than 30 Hz, while in the EEG the band is contained at frequencies lower than 30 Hz. By indicating with f_t the frequency that separates the EEG band from the EMG band, f_s the sampling frequency and p_1 and p_2 the powers relative to the bands $[0 f_t]$ and $[0 f_s/2]$, we can evaluate the ratio $r = p_1/p_2$. Based on the value of the latter, components that are less than a certain value will be considered components of muscular electrical activity.

Such as the EOG artifact, the EEG signal $\hat{x}(t)$ can be reconstructed by multiplying the signal itself with the mixing submatrix A_{EMG} which contains only the neural sources (no artifacts) and its pseudoinverse matrix $A_{EMG}^\#$ [19]:

$$\hat{x}(t) = A_{EMG}A_{EMG}^\#x(t) \quad (3.2)$$

According to [18], for impulsive artifacts such as EMG, it is preferable to use epochs of short duration. In this regard, epochs of 3 seconds were used, while the f_t frequency and the ratio r were set at 15 Hz and 10 respectively. EMG removal was applied to the same 10 second signal segment used previously. The result is shown in figure 3.2.

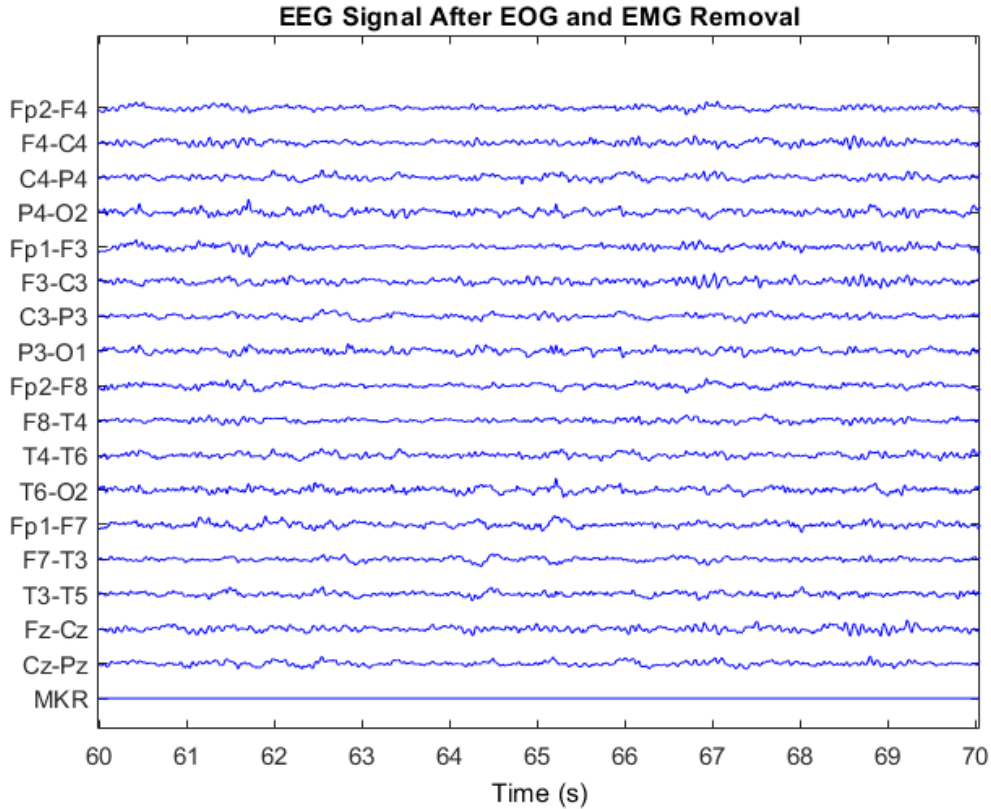


Figure 3.6: 10 seconds of EEG signal after EMG removal

3.3 Algorithm

After having cleaned the signals from the artifacts that could compromise the goodness of the work, it is possible to apply the algorithm that can be summarized in three steps:

1. Construction of prototype waves that best represent a mathematical model suitable for representing pathological waveforms.
2. Calculation of matched filters through a normalized cross-correlation, between each channel and each waveform.
3. Of the waves found in the previous step, only those with an amplitude greater than a noise threshold were kept.

The algorithm was implemented in MATLAB.

3.3.1 Prototype Waveforms Construction

For each EEG signal described in [3.1](#), the spike and waves identified by a neurologist were provided. These spike and waves were then fitted in order to identify a mathematical model able to best describe them.

As a result of the fitting, the *sinc* function was chosen to model the spike and a *gaussian* function to model the wave after the spike. Subsequently, both the functions created were windowed through a rectangular window; in the case of the *sinc*

the window is centered in correspondence with the spike, in the case of the wave the window is shifted to the right to maintain the *gaussian* peak and its final part. In particular the two functions are:

$$\text{sinc}(t) = \begin{cases} \frac{\sin(\pi t)}{\pi t} & t \neq 0 \\ 1 & t = 0 \end{cases} \quad (3.3)$$

which can also be written in the analytic form:

$$\text{sinc}(t) = \frac{1}{2\pi} \int_{-\pi}^{\pi} e^{j\omega t} d\omega \quad (3.4)$$

The latter corresponds to the continuous inverse Fourier transform of a rectangular pulse.

As for the *gaussian* instead it was used in the form:

$$g(t) = ae^{-\frac{(t-b)^2}{c^2}} \quad (3.5)$$

which can be rewritten in the form:

$$g(t) = \frac{1}{\sigma\sqrt{2\pi}} e^{-\frac{(t-\mu)^2}{2\sigma^2}} \quad (3.6)$$

with μ is the mean and σ is the standard deviation of the distribution. By varying these parameters it was possible to change the wave, which compared to the spike, is the one that most highlighted changes in the fitted data.

For the spike, duration values between 30 and 100 ms were chosen, while for the wave the times were varied from 100 to 300 ms. An example of the prototype obtained is shown in the figure [3.7](#). Moreover, another feature chosen to obtain spike

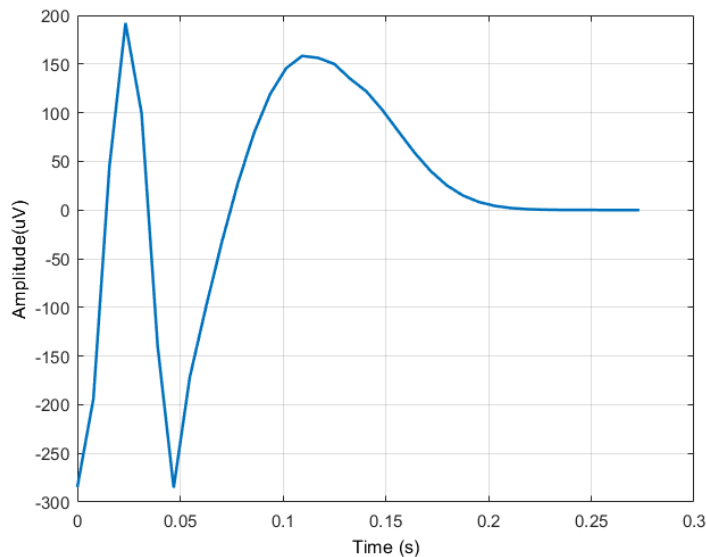


Figure 3.7: Prototype waveform

and waves patterns was the amplitude ratio between spike and wave $\frac{A_{SPIKE}}{A_{WAVE}}$, In fact, the spike does not always have a greater amplitude than the wave.

For this reason, by varying $\frac{A_{SPIKE}}{A_{WAVE}}$, a total of 17 prototypes waveforms shown in the figure 3.8 were obtained. Note that the first five prototypes are actually more like

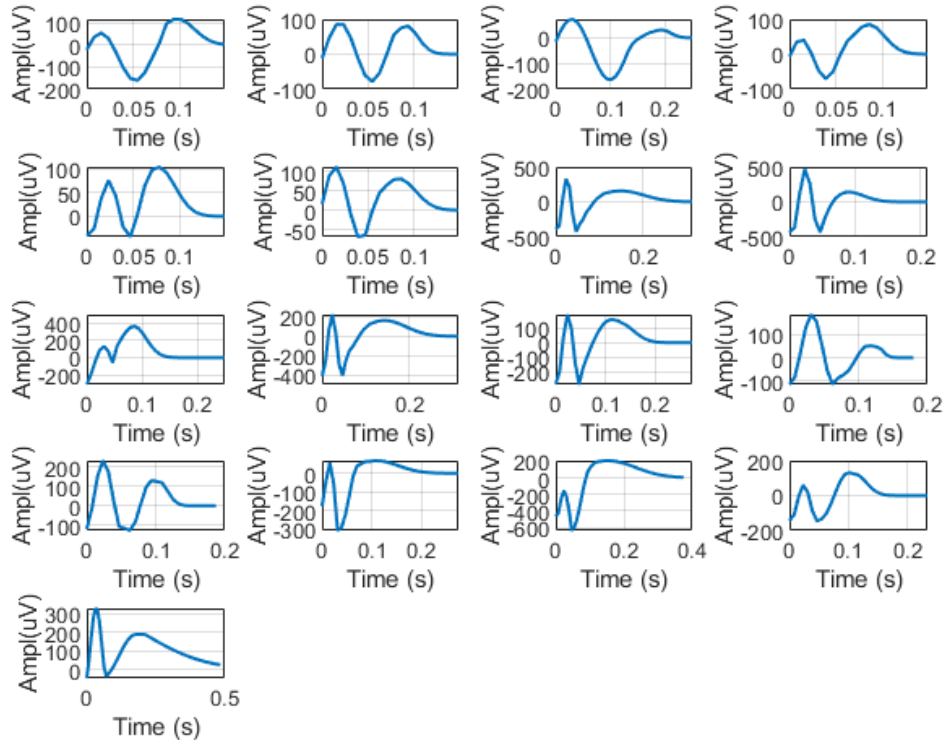


Figure 3.8: Set of prototypes

spikes and sharp waves than spike and waves. It is necessary because these types of waveforms are also characteristic of epilepsy and as such have been highlighted by the neurologist.

3.3.2 Calculation of the Normalized Cross-Correlation

After finding mathematical models that could best approximate the spike and waves identified by the neurologist, a set of match filters between each prototype and EEG channel was applied. In particular, the normalized cross-correlation was computed [20]:

$$C(t) = \frac{\int x(\tau)w(t + \tau)d\tau}{\| x \|_2 \| w \|_2} \quad (3.7)$$

$x(t)$ and $w(t)$ are the EEG channel and the prototype waveform respectively, while $\| \cdot \|_2$ indicates the root mean square (RMS) of the argument. Therefore, in this case, the cross-correlation (which is constituted by the numerator of equation 3.7) is divided by the energy (RMS) of the signal and of the prototype (normalization is performed). In particular, the energy of the signal that is used is only the portion of the signal that overlaps the prototype when the cross-correlation is performed. In detail in MATLAB, this is achieved by means of a convolution (which is implemented in MATLAB by the Fast Fourier Transform algorithm) between the squared

signal and a rectangular window equal to the length of the prototype (this allows to zero all the signal except the piece that is compared with the prototype). In fact, the convolution already performs a sum, so that the energy of the signal is obtained in the portion in which it is superimposed on the prototype. The energy of the prototype, on the other hand, is always constant. The numerator instead is obtained simply through the convolution between the EEG channel and the translated prototype.

Due to the normalization of the cross-correlation with the energies of the prototype and of the signal, cross-correlation values obtained vary between -1 and 1. A value equal to -1 is obtained when the signal portion coincides perfectly with the reversed prototype $-w(t)$. On the other hand, a value equal to 1 is obtained when the signal portion coincides perfectly with the prototype $w(t)$. Clearly, since the prototypes are mathematical models reconstructed by fitting real spike and waves, cross-correlation values equal to 1 or -1 will never be obtained.

Furthermore, even if there is a signal waveform identical to the prototype, the maximum cross-correlation will not be obtained due to possible artifacts, electrodes interference, electronic noise, etc. Thus, a normalized cross-correlation threshold at 85% was chosen, which was compared to its absolute value. A value higher than the threshold indicates a match with between the prototype and the analyzed signal portion, so it will be taken into consideration for subsequent processing. A value lower than the threshold, on the other hand, indicates a match that is not sufficiently high, so that the portion of the signal identified will be discarded. An example of cross-correlation between a channel and a prototype is shown in the figure [3.9](#). In this window there are two matches, i.e. two values above the threshold which indicate a high cross-correlation between signal and prototype in that instant of time.

The choice to normalize the cross-correlation allows to take into account only the ratios between the amplitude of the spike and the wave and not the absolute amplitudes. This way any waveform that resembles the prototype with a cross-correlation value beyond the threshold is considered. Therefore, even spike and waves of much smaller amplitude than those of the prototypes were selected as potential spike and wave. For this reason, after carrying out the normalized cross-correlation between each prototype and each EEG channel, each waveform identified was subjected to another threshold [21](#). Assuming σ_n the standard deviation of the noise:

$$\sigma_n = \text{median} \left\{ \frac{|x|}{0.6745} \right\} \quad (3.8)$$

where x is the channel considered. The amplitude threshold for the previously identified waveforms was set at 5 times the value of [3.8](#):

$$Th = 5\sigma_n \quad (3.9)$$

Thus, all waveforms with amplitude less than the threshold were excluded. The use of the threshold [3.9](#) allows to consider the fact that according to the considered channel the level of background activity can change. Indeed, given that the spike and wave are waveforms that are clearly distinguished from the background activity

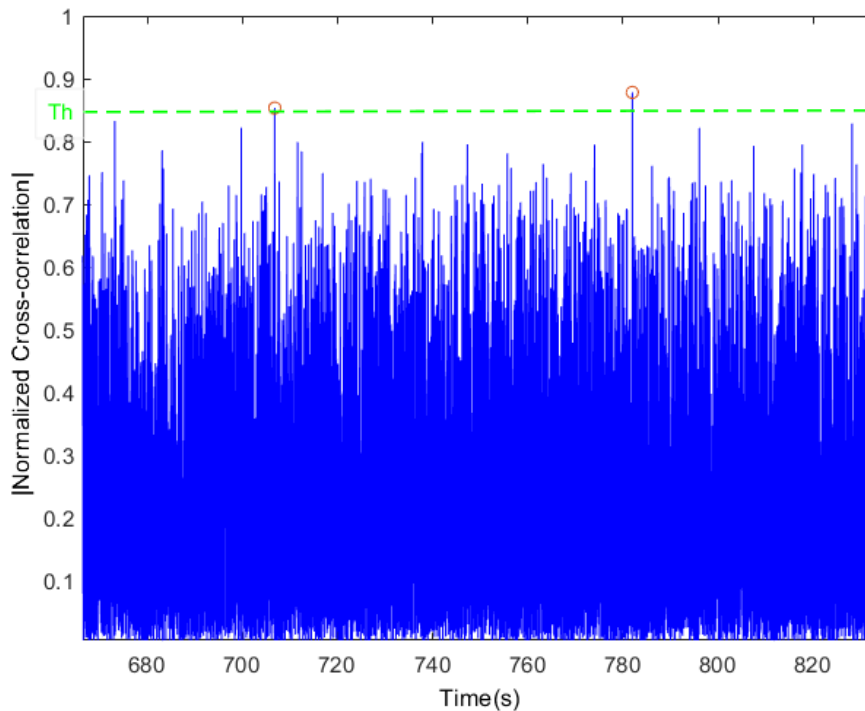


Figure 3.9: Absolute value of normalized cross-correlation

as explained in [1.2.2](#), the threshold allows to distinguish what is background from what is not.

So, in summary, after detecting the most prototypes-like waveforms from each EEG channel, each of them was subjected to amplitude control based on the background activity threshold of the EEG channel in which the waveform is located. Given the great variability of spike and wave shape, it is possible, even if rarely, that the same waveform of the signal can be selected from more than one prototype. For this reason, a control has been inserted that if identical waveforms are detected, only one is kept and the others are eliminated.

Finally, a check was made on the instants of time and on the channels in which the waveforms were identified. In fact, since the source of the seizure cannot be found only in one of the channels, all the waveforms visible in a single channel have been discarded, as sporadic and non-epileptic index. The location of the waveform is very important. For example, if the waveform was found in a frontal electrode, then it is very likely that it is also detected in the adjacent electrodes, rather than for example in occipital electrodes. For this reason, more weight has been given to the waveforms present in adjacent electrodes, compared to electrodes far from each other.

Examples of waveforms identified by the algorithm is shown below. Waveforms that have a high normalized cross-correlation with the signal are shown in green. Specifically in the figure [3.10](#) a 20 seconds epoch of an EEG signal is represented

including all the channels in which the waveforms identified are noted, while in [3.11](#) a spike and wave complex is represented, that is a consecutive series of spike and waves typically present during the seizure.

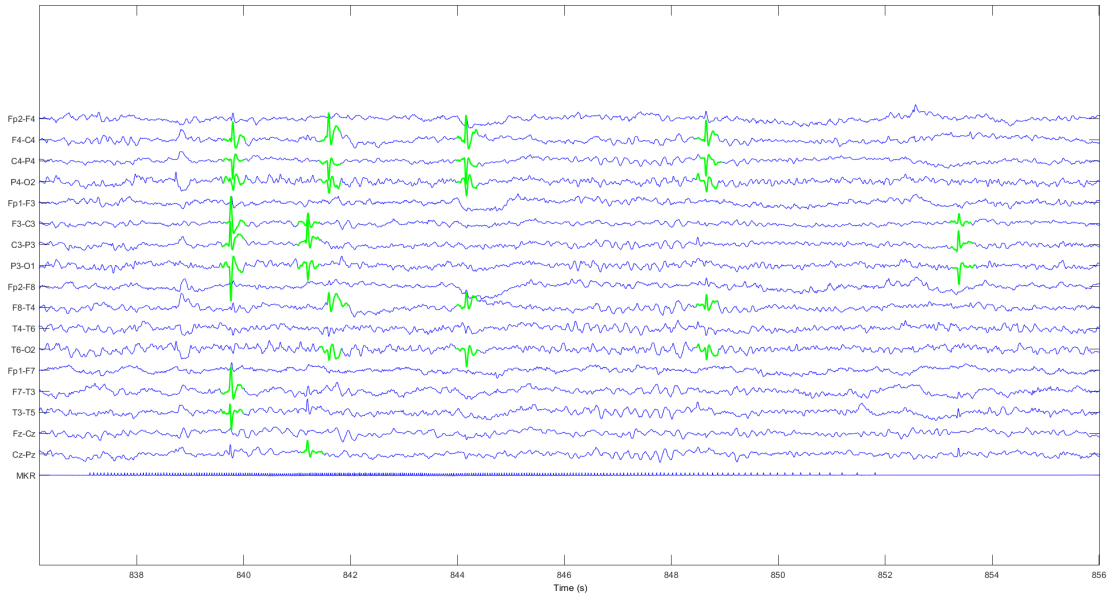


Figure 3.10: Waveforms identified in 20 seconds of original EEG epoch

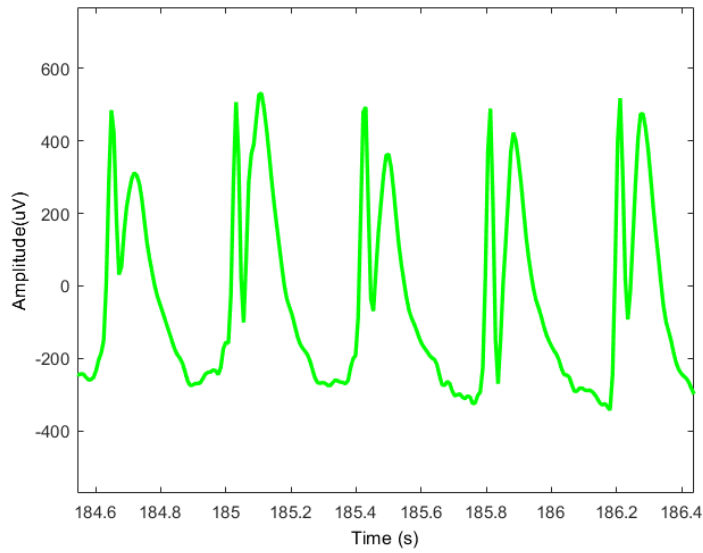


Figure 3.11: Spike and wave complex identified by the algorithm

Chapter 4

Results

4.1 Evaluation of Algorithm Results

To evaluate the algorithm's ability to correctly recognize the waveforms identified by the neurologist, as a first step, the following are defined:

- **true positive (TP)** - the spikes / spikes and waves that are present in the signal and that are also detected by the algorithm;
- **true negative (TN)** - the spikes / spikes and waves that are not present in the signal and that the algorithm does not detect, in this case it is not possible to define a value of TN;
- **false positive (FP)** - waveforms that have been detected as spikes / spike and waves by the algorithm but are not really spikes / spike and waves;
- **false negative (FN)** - real spikes / spike and waves that are not identified by the algorithm while they have been identified by the neurologist.

In this validation it was not possible to calculate specificity and accuracy, as it was not possible to define the true negatives. The measures used to evaluate performance are:

- **sensitivity or true positive rate (TPR)**

$$TPR = \frac{TP}{TP + FN} \quad (4.1)$$

which is a measure of the algorithm's ability to correctly identify the waveforms identified also by the neurologist and is given by the ratio between the true positives and the totality of waveforms identified by the neurologist;

- **precision or positive predictive value (PPV)**

$$PPV = \frac{TP}{TP + FP} \quad (4.2)$$

which defines the probability that a waveform identified by the algorithm is actually a pathological waveform;

- **miss rate or false negative rate (FNR)**

$$FNR = \frac{FN}{FN + TP} \quad (4.3)$$

which is the ratio between true waveforms not detected by the algorithm and the total of true waveforms;

- **false discovery rate (FDR)**

$$FDR = \frac{FP}{FP + TP} \quad (4.4)$$

which indicates how much the algorithm detects false positives out of the total of positives.

These measurements were made in the first 444 seconds of each dataset signal [3.1](#). The values are reported in the table [4.1](#).

Patient	TPR	PPV	FNR	FDR
1	0.93	0.81	0.07	0.19
2	0.92	0.92	0.08	0.08
3	1	0.68	0	0.32
4	0.89	0.84	0.11	0.16
5	0.55	0.63	0.45	0.37
6	0.85	0.51	0.15	0.49
7	0.98	0.81	0.02	0.19
8	1	0.2	0	0.8
9	0.87	0.79	0.13	0.21
10	0.45	0.42	0.55	0.58
Mean	0.85	0.67	0.15	0.33
Std	0.19	0.22	0.19	0.22

Table 4.1: Evaluation of algorithm results

The table shows a consistently high sensitivity with the exception of two patients (5 and 10). In fact, by eliminating these two patients a sensitivity is achieved on average equal to 93%. By eliminating the same patients, the PPV rises to 70%. This means that the algorithm is good at identifying true positives even though there are often false positives in a considerable number.

4.2 Clinical Applications

After testing the algorithm, it is preceded to use it in some clinical applications which will be discussed below.

4.2.1 Comparison With Healthy Patients

To understand if the algorithm was able to distinguish a healthy patient from an epileptic patient, it was tested on 10 healthy patients, for a total EEG trace of about 5 hours and 23 minutes. These were compared with epileptic patients whose dataset was described in [3.1]. In particular, the number of spikes and waves per second that were found by the algorithm in signals belonging to healthy patients and in signals belonging to epileptic patients was calculated. The comparison between the two averages is shown in the figure [4.1].

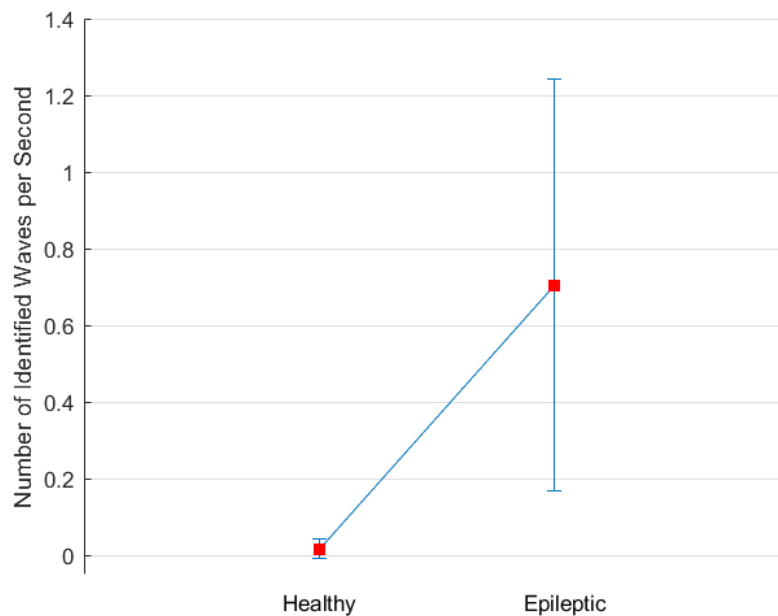


Figure 4.1: Difference between number of waves per second identified by algorithm

The number of waves per second of healthy patients is equal to 0.017 ± 0.025 , while for epileptic patients is equal to 0.705 ± 0.537 . To understand if the number of waves per second had a statistical difference, the Wilcoxon signed-rank test (a non-parametric test that does not require the hypothesis of Gaussianity of the distributions) was applied on the two distributions of healthy patients and epileptic patients. As was to be expected, the two distribution of waves per second of the two categories of patients have an highly significant differences ($p = 4.1135e^{-5}$).

The few waveforms found in healthy patients are therefore waveforms that closely resemble the prototypes shown in figure [3.8] but their frequency is significantly lower than the frequency at which they are identified in epileptic patients. Furthermore, as can be seen from the distribution of the amplitudes of the two patient categories in the figure [4.2] It is noted that the amplitudes of the waveforms identified in healthy

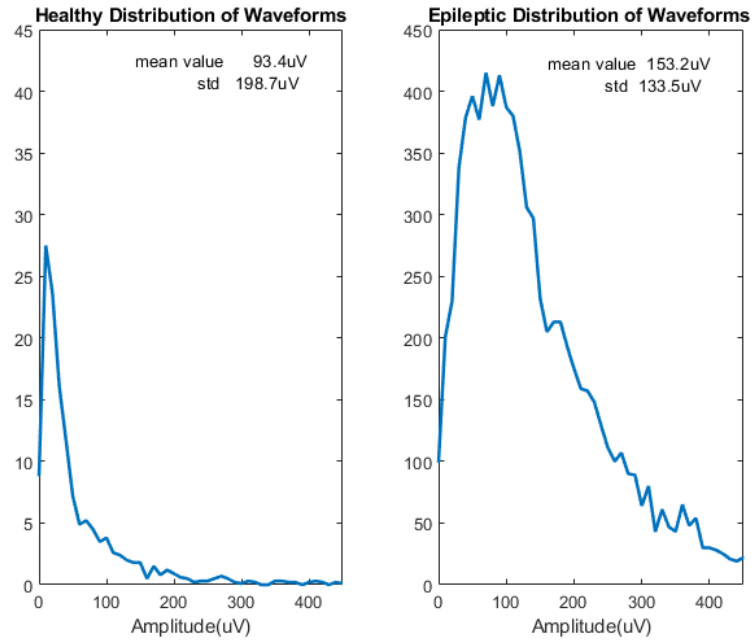


Figure 4.2: Difference between amplitude distributions

patients are lower than in epileptic patients. This may justify that the waveforms found are only similar in shape to the prototypes but the amplitudes are lower. This is due to the fact that in [3.3.2](#) the cross-correlation as well as being divided by the energy of the prototype, is also divided by the portion of the signal that overlaps the prototype and also the amplitude threshold ([3.9](#)) is not an absolute threshold but depends on the channel considered.

4.2.2 Comparison With ADHD Patients

Another comparison was made with respect to ADHD patients (attention deficit hyperactivity disorder). ADHD is a prevalent disorder in young children. It includes difficulties in attention and concentration, impulse control and level of activity. These problems essentially derive from the child's inability to regulate their behavior according to the passage of time, the objectives to be achieved and the demands of the environment [22]. Some studies [23] [24] have shown that typical abnormalities of the eeg signals of epileptic patients can be found in the eeg signals of ADHD patients, so much so that they are often control to understand if epilepsy as commorbidity may occur. At the same time, epileptic patients can also develop ADHD. These results show that ADHD is a condition in which abnormalities in the EEG signal can be seen which, at times, are similar to epileptic activity; for this reason the algorithm was also tested on a sample of 8 patients diagnosed with ADHD. An example of waveforms identified by the algorithm in a signal from an ADHD patient is shown in the figure 4.3. Note that the detected waveforms are actually more like

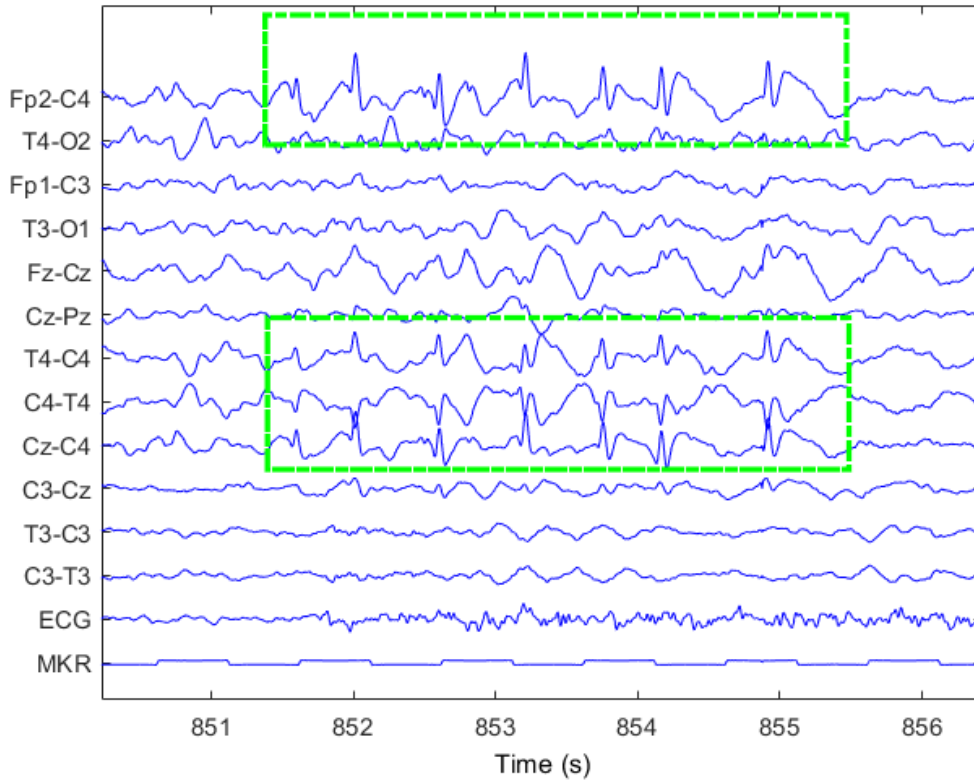


Figure 4.3: Waveforms identified in ADHD patient

spikes or sharp waves than spikes and waves.

For each ADHD patient, the number of waveforms per second identified was calculated and compared to healthy and epileptic patients. In the figure 4.4 you can see that there is always a notable difference between epileptics and the other two categories. However, comparing the number of waveforms per second of ADHD patients (0.069 ± 0.035) with that of healthy patients (0.017 ± 0.025), it is noted that there is a difference between the two categories, confirming that even in ADHD patients it

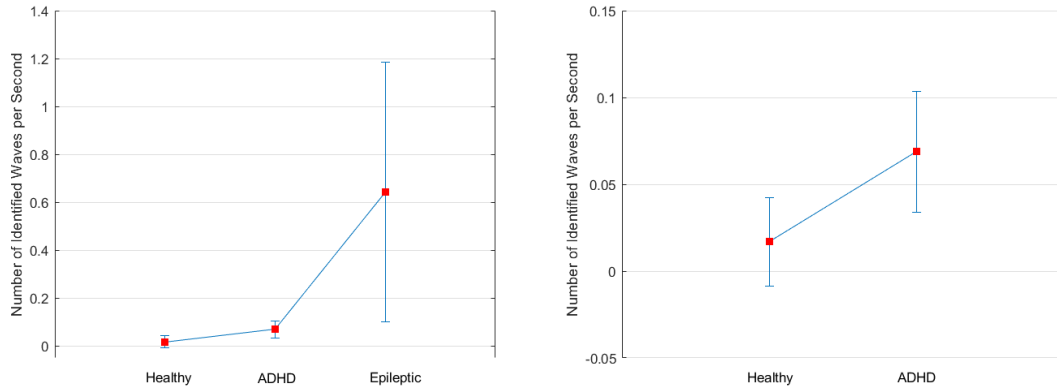


Figure 4.4: Difference between number of identified waves per second

is possible to find waveforms similar to those that can be found in epileptic patients. The Wilcoxon signed-rank test was applied on the two distributions of healthy patients and ADHD patients, obtaining a p -value equal to 0.0055 (highly significant differences).

Observing the distributions of the amplitudes in the figure [4.5](#), it can be seen that the values of the amplitudes of ADHD are similar to those of epileptic patients, while it was not so for healthy patients. This confirms that the waveforms are indeed similar between the two categories of patients.

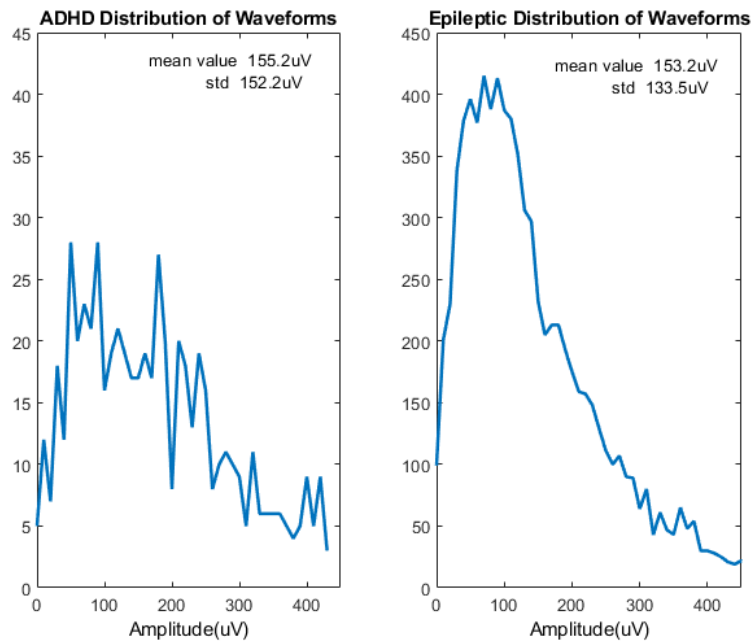
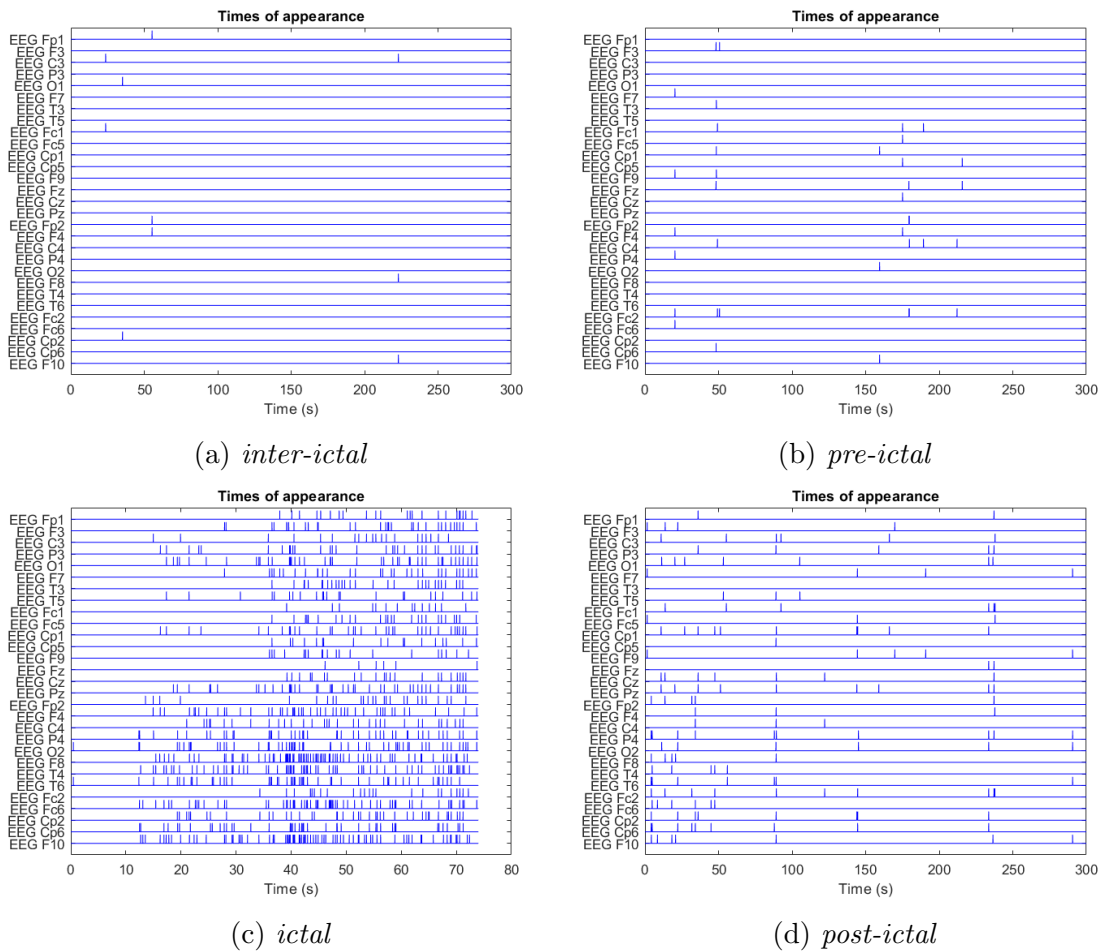


Figure 4.5: Difference between amplitude distributions

4.2.3 Temporal and Spatial Distribution

We wanted to investigate if the waveforms identified by the algorithm had any influence on the epileptic seizure and also if they had a relationship with the positioning of the epileptic focus. To carry out these analysis, the dataset [3.1](#) could not be used, because first of all they are patients with induced epilepsy, therefore the number and frequency of spikes can be influenced; secondly, because it is generalized epilepsy, for which there is no indication of the epileptic focus and for which it is not possible to carry out this analysis.

For these reasons, from the website [25](#), five recordings were used at different times of a patient with (non-induced) right temporal lobe epilepsy. Each recording was then divided into four different periods: *inter-ictal*, *pre-ictal*, *ictal* and *post-ictal* as described in [1.2](#); in particular for the pre and post seizure a period of 5 minutes was considered. An example of time of appearance relating to recording 4 of each period is shown in the figure [4.6](#).



waves per second identified by the algorithm in each period is shown in the figure [4.7](#).

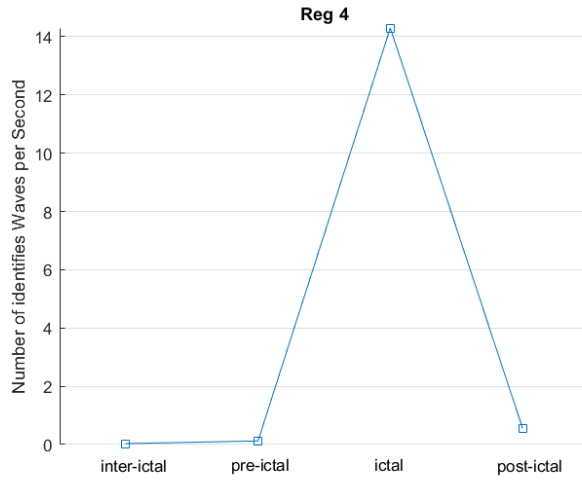


Figure 4.7: Number of identified waves per second in each period

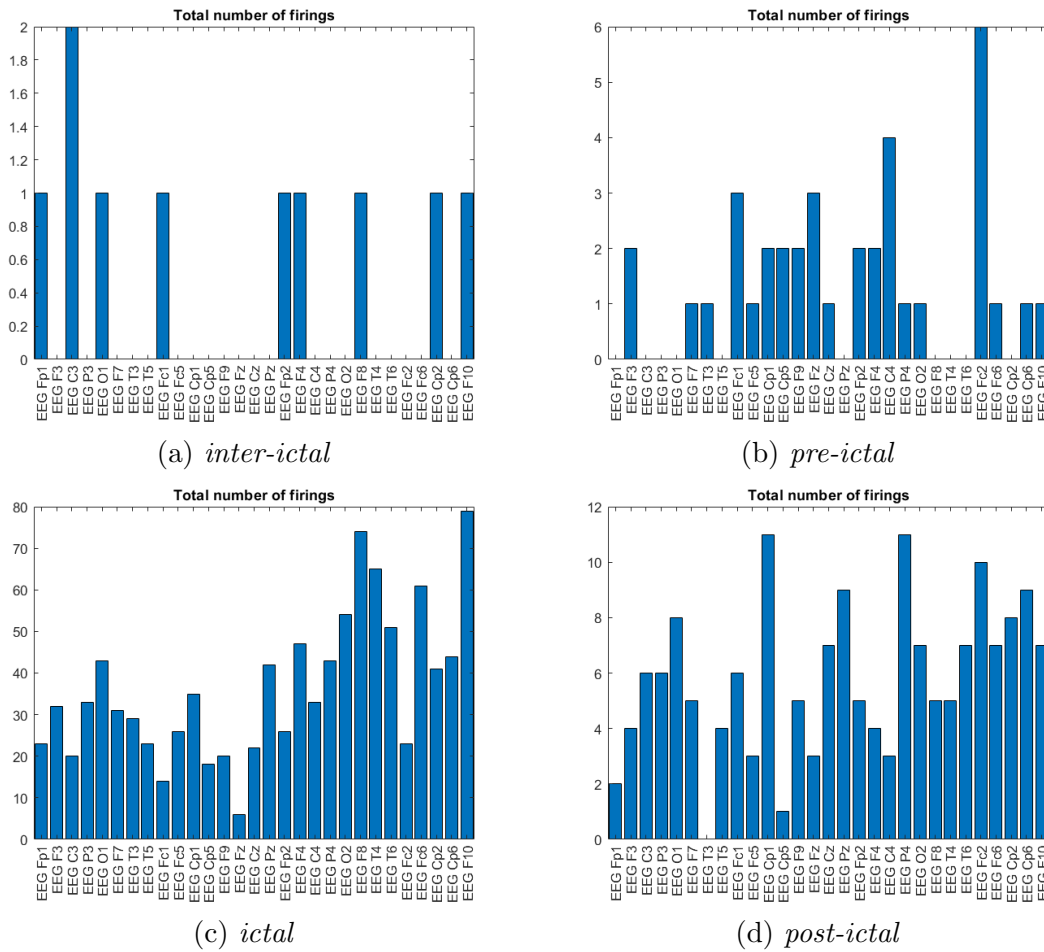


Figure 4.8: Distribution in each period

As for the number of waveforms identified in each EEG channel in each period, it is noted that the number is greater during the seizure. Furthermore, the channels in

which the greatest number of waves are found are those relating to the right temporal lobe or in proximity to it. However, this can only be said for what concerns the distribution during the seizure (*ictal* period), while for the other periods there is no clear concentration of the waveforms in the channels relative to the right temporal lobe, so it is not possible to say that the positioning of the spikes (with the exception of the seizure period) is in correlation with the epileptic focus.

As can be seen better in the figure 4.9, which shows the distribution over the scalp computed by interpolation, the highest number of waves per second coincides with the localization of the epileptic focus only during the seizure. Note how the order of magnitude is also profoundly different between one period and another because there are more pathological waveforms during the seizure respect to other periods.

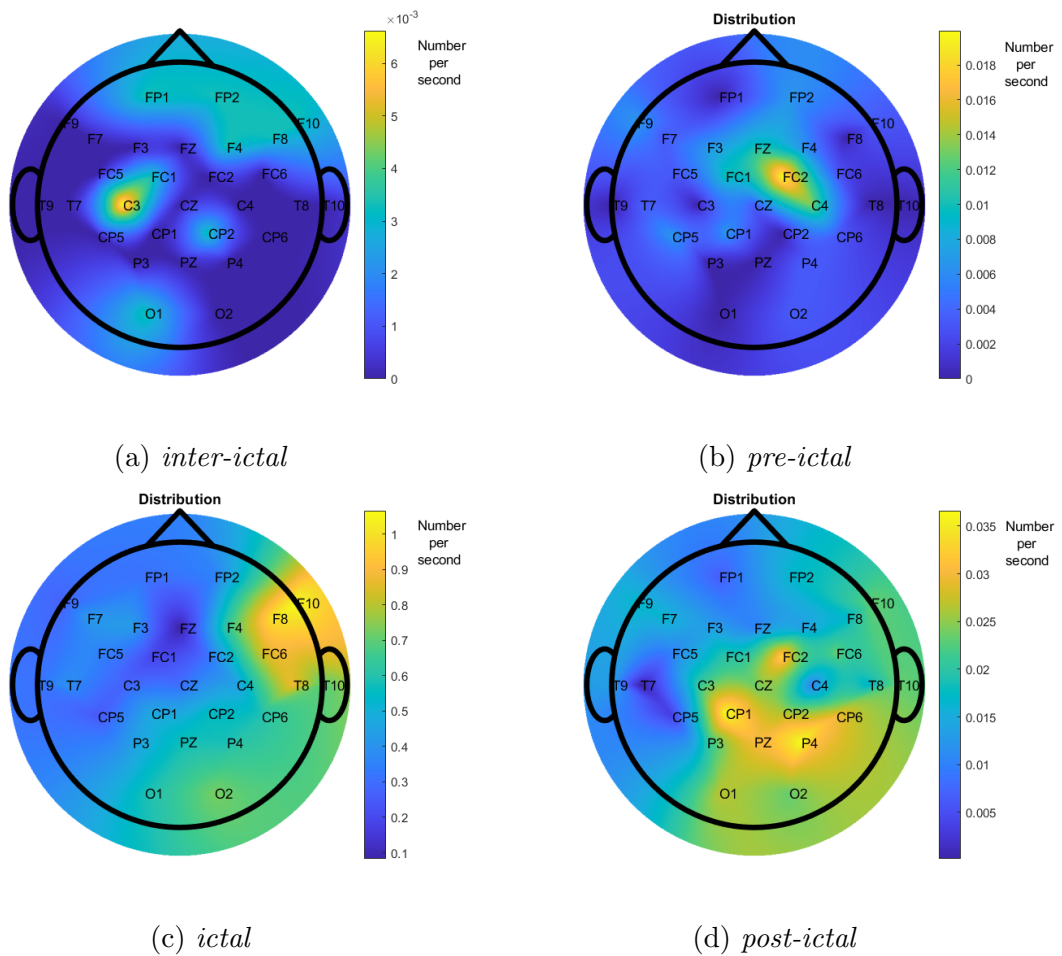


Figure 4.9: Distribution over the scalp in each period

The non-correlation, with the exception of the *ictal* period, between the number of waves per second and epileptic focus, may be due to the fact that if the focus is located in a deep area of the brain, it is not always possible to associate the epileptogenic activity also in the surface (where the signal is picked up).

This applies to all five patient records. As can be seen from the boxplot in the figure 4.10, which represents the number of waveforms per second identified in each period

for the total number of registrations (all five are taken into account), it is clear that the number of waves per second is higher during the seizure (*ictal*) than in the other periods. Furthermore, before and after (precisely 5 minutes before and 5 minutes

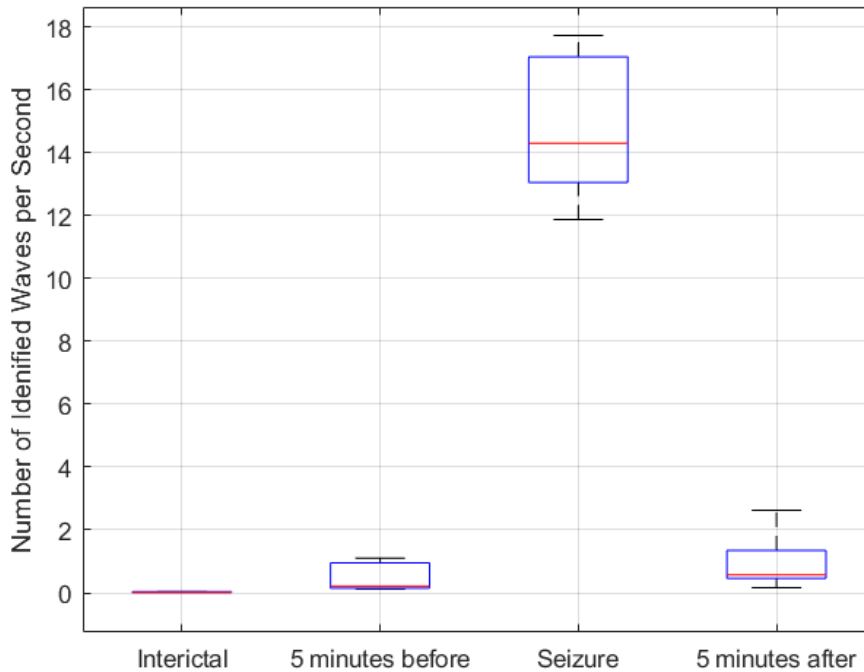


Figure 4.10: Number of identified waves per second in each period (Boxplot)

after) the seizure, the number of waveforms per second is higher than in the period away from the seizure (*inter-ictal*). However, having only a number as an index to identify a period, it is not possible to understand if there is a significant statistical difference between each period.

For this reason, all the delays between two consecutive spikes were calculated to have a distribution of delays pertaining to the *inter-ictal* period, one for the *pre-ictal* period, one for the *ictal* and finally one for the *post-ictal*. In this way it is also possible to understand if there is a correlation between the increase in the frequency of firings and the onset of the epileptic seizure. As can be seen from the figure [4.11](#), which represents the trend of delays between two consecutive spikes for each period and for each recording, it is noted how, for all the recordings, there is a substantial decrease in the delays (i.e. an increase in the frequency of firings) between *inter-ictal* and *pre-ictal*, then, during the seizure, the delays decrease and then increase again during the *post-ictal* period. The difference between *inter-ictal* and *pre-ictal* is very important since a considerable variation in frequency could be used as a method for predicting the seizure. Considering the figure on the right of [4.11](#), which represents the average delay of each period, taking into consideration the totality of the delays, we have that for the *inter-ictal* period the average delay is equal to 244.71 s, with a standard deviation of 56.63 s. In the *pre-ictal* period the average delay is equal to 30.02 s, while the standard deviation is 39.65 s. During the *ictal* period, however, the average delay is greatly reduced to 1.4 s, with a standard deviation of 1.87

s. Finally, in the *post-ictal* period the delay increases again to 25.65 s, while the standard deviation is 37.74 s.

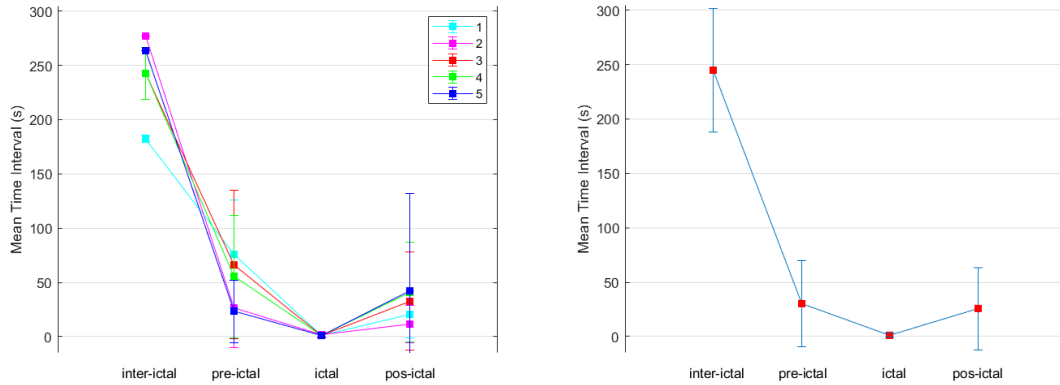


Figure 4.11: Mean time interval variation in each trace (left) and in total (right)

Time intervals obtained in each period are compared in the boxplots in [4.12](#). It's possible to observe the difference between the median of each period. In the *inter-ictal* period there are high values, which decrease in the *pre-ictal* period. In the *ictal* period these values decrease further and then grow back to a value comparable to the *pre-ictal* period during the *post-ictal* period. Using a boxplot of type notch

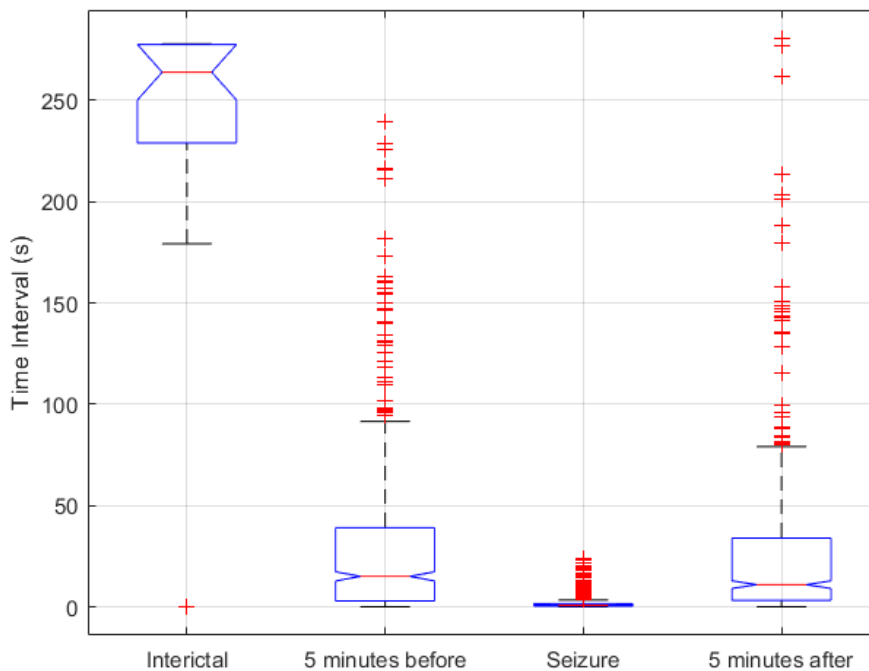


Figure 4.12: Delays in each period (Boxplot)

it is possible to say that there is a significant statistical difference because the test confidence intervals are not overlapping, especially between *inter-ictal* and *pre-ictal* period. Furthermore, it is noted that before and after the seizure, the intervals are more variable than the *inter-ictal* or *ictal* period.

The Wilcoxon signed-rank test was applied to test the significant differences between the delays distributions of each period. In all cases (5 records) there is a p -value of less than 0.05, which demonstrates a high statistical difference between each period. What is most interesting is the difference between *inter-ictal* period and *pre-ictal* period in order to predict the seizure.

Chapter 5

Conclusions and Future Work

The detection of spike and waves in patients suffering from epilepsy is a useful tool for diagnosis and therapy, in particular the automatic identification can be a helpful support for the neurologist to reduce the analysis time of the EEG traces. In fact, especially for long duration signals such as EEG holter, the time needed to analyze the whole signal is a lot, so an instrument that allows, in a few seconds, to analyze an entire trace could be very useful.

In this study a fast method has been introduced, capable of being used also in real-time, which is able to identify spike and waves through the normalized cross-correlation between the signal and a set of accurately constructed mathematical models. The sensitivity achieved is 85% but, by eliminating two patients, the sensitivity reaches 93%, although still lower than other automatic identification methods such as [26] and [27]. In these patients, there are few wave spikes in the seconds analyzed, and they also appear to be morphologically slightly different. The main problem of the method adopted is in fact that it strictly depends on the shape of the waveforms to be analyzed. A slight variation in the shape could lead to incorrect identification of the waveform. For this reason, it is necessary to introduce new prototypes obtained with more accurate mathematical models to be used in cross-correlation. It is also important to keep in mind the type of montage considered: these prototypes were created considering a bipolar assembly and were tested on bipolar signals. The shape in monopolar signals in common reference does not change the shapes of waveforms much while monopolar signals with average reference could be a problem because the shape of the spikes is different. Another problem related to the algorithm and which could be improved is the fact that sometimes it is able to identify the spike but not the wave or vice versa. Again, a better construction of the prototypes could lead to a resolution of the problem. Improvements could also be made regarding the threshold used: there are rarely spikes that get confused with the background activity. Given the threshold that allows you to take waveforms that are distinguished from the background activity, the previous waves are lost.

Despite this, however, the results are encouraging. As for the clinical applications discussed, it has been shown that the algorithm is able to distinguish between a healthy patient and a sick one and is also specific for spike and waves as they are also found in EEGs where they are present (ADHD patients) but in smaller numbers. compared to EEG of epileptic patients. Encouraging results were obtained

by analyzing the temporal distribution of the spikes. To do this [25] has been used, the data consisting of five recordings in different periods of the same patient suffering from epilepsy. In all cases it was noted that in correspondence with the seizure there is an increase in the number of spikes and an increase in their frequency. It was more interesting to note that the increase in number and frequency also changes between the *inter-ictal* and *pre-ictal* periods, in fact in correspondence with the *pre-ictal* there is an increase in both. As for the spatial distribution, no correlation was noted between the positioning of the tips and epileptic focus except for the period during the attack. This can be explained by the fact that the epileptic focus is often found in depth so that, since the electrodes are placed on the surface in the scalp, it is difficult to precisely collect the signal. It is important to underline that this study was carried out on one patient (albeit on several recordings) and for this reason a larger dataset would be needed. Furthermore, the presence of spikes is also related to the type of epilepsy, so having patients with different epilepsy would be useful.

Future studies could be conducted to understand if, based on the number and frequency of spikes, there is a threshold that alarms the doctor and for which it is decided to act pharmacologically in order to prevent the crisis as in [28]. Or even based on the number and frequency, being able to figure out what is the right dose of the drug. It would be interesting, given the evidence found in ADHD patients, to understand when they may be considered at risk of epilepsy simply based on the incidence of spikes in the EEG, looking for a parameter that allows to discriminate those who are at risk and which are not. All of these are interesting studies that are projected to improve people's health.

Bibliography

- [1] Eddie Johnson Jody e. Johnson Oksana Korol Dean Kruse Brandon Poe James A. Wise Mark Womble Kelly A. Young J. Gordon BETTS Peter Desaix. *Anatomy and Physiology*. Ed. by OpenStax. OpenStax, 2017 (cit. on p. 11).
- [2] Oregon State University. *Structure and Function of the Nervous System*. URL: <https://open.oregonstate.edu/aandp/chapter/12-1-structure-and-function-of-the-nervous-system/> (cit. on p. 12).
- [3] Teach Me Physiology. *Action Potential*. URL: <https://teachmephysiology.com/nervous-system/synapses/action-potential/> (cit. on p. 14).
- [4] Ingrid Scheffer, Samuel Berkovic, Giuseppe Capovilla, Mary Connolly, Jacqueline French, Laura Guilhoto, Edouard Hirsch, Satish Jain, Gary Mathern, Solomon Moshe, Douglas Nordli, Emilio Perucca, Torbjörn Tomson, Samuel Wiebe, Yue-Hua Zhang, and Sameer M Zuberi. “ILAE classification of the epilepsies: Position paper of the ILAE Commission for Classification and Terminology”. In: *Epilepsia* 58 (Mar. 2017). DOI: [10.1111/epi.13709](https://doi.org/10.1111/epi.13709) (cit. on p. 19).
- [5] Joseph Roger, Fritz Dreifuss, Manuel Martinez-Lage, Claudio Munari, Roger Porter, Masakazu Seino, Peter Wolf, Jean Bancaud, Patrick Chauvel, A. Escueta, Jerome Jr, Richard Mattson, Timothy Pedley, J. Penry, L. Quesney, and Heinz Wieser. “Proposal for Revised Classification OF Epilepsies and Epileptic Syndromes”. In: *Epilepsia* 30 (Apr. 1989), pp. 389–399. DOI: [10.1111/j.1440-1819.1985.tb02013.x](https://doi.org/10.1111/j.1440-1819.1985.tb02013.x) (cit. on p. 19).
- [6] O. Mecarelli. *Manuale teorico pratico di elettroencefalografia*. 2009 (cit. on p. 20).
- [7] Maxim Bazhenov, Igor Timofeev, Flavio Frohlich, and Terrence Sejnowski. “Cellular and network mechanisms of electrographic seizures”. In: *Drug discovery today. Disease models* 5 (Feb. 2008), pp. 45–57. DOI: [10.1016/j.ddmod.2008.07.005](https://doi.org/10.1016/j.ddmod.2008.07.005) (cit. on p. 22).
- [8] Ivan Cohen, Vincent Navarro, Stéphane Clemenceau, Michel Baulac, and Richard Miles. “On the Origin of Interictal Activity in Human Temporal Lobe Epilepsy in Vitro”. In: *Science (New York, N.Y.)* 298 (Dec. 2002), pp. 1418–21. DOI: [10.1126/science.1076510](https://doi.org/10.1126/science.1076510) (cit. on p. 22).
- [9] Richard Ngomba, Ines Santolini, Thomas Salt, Francesco Ferraguti, Giuseppe Battaglia, Ferdinando Nicoletti, and Gilles van Luijtelaaar. “Metabotropic glutamate receptors in the thalamocortical network: Strategic targets for the treatment of absence epilepsy”. In: *Epilepsia* 52 (May 2011), pp. 1211–22. DOI: [10.1111/j.1528-1167.2011.03082.x](https://doi.org/10.1111/j.1528-1167.2011.03082.x) (cit. on p. 22).
- [10] info medics. URL: <https://www.infomedics.it/therapeutic-areas/epilessia/diagnosi.html> (cit. on p. 22).

- [11] Luca Mesin, Ales Holobar, and Roberto Merletti. “Blind Source Separation: Application to Biomedical Signals”. In: June 2011, pp. 379–409. ISBN: 9780470422144. DOI: [10.1002/9781118007747.ch15](https://doi.org/10.1002/9781118007747.ch15) (cit. on pp. [25](#), [26](#)).
- [12] L. Mesin. *Neuromuscular System Engineering*. La community di ilmiolibro.it. ilmiolibro self publishing, 2019. ISBN: 9788892361881. URL: <https://books.google.it/books?id=B9eFygEACAAJ> (cit. on pp. [25](#), [26](#)).
- [13] Shashank Chauhan. “Second Order Blind Source Separation techniques (SO-BSS) and their relation to Stochastic Subspace Identification (SSI) algorithm”. In: vol. 3. June 2011, pp. 177–187. ISBN: 978-1-4419-9833-0. DOI: [10.1007/978-1-4419-9834-7_16](https://doi.org/10.1007/978-1-4419-9834-7_16) (cit. on p. [26](#)).
- [14] Wim Clercq, Anneleen Vergult, Bart Vanrumste, Wim Paesschen, and Sabine Huffel. “Canonical Correlation Analysis Applied to Remove Muscle Artifacts From the Electroencephalogram”. In: *IEEE transactions on bio-medical engineering* 53 (Jan. 2007), pp. 2583–7. DOI: [10.1109/TBME.2006.879459](https://doi.org/10.1109/TBME.2006.879459) (cit. on pp. [27](#), [35](#)).
- [15] John C. Bancroft. “Introduction to matched filters”. In: 14 (2002) (cit. on pp. [28](#), [29](#)).
- [16] Catherine Stamoulis and Andrew Richardson. “Application of matched filtering to identify behavioral modulation of brain oscillations”. In: *Journal of computational neuroscience* 29 (June 2009), pp. 63–72. DOI: [10.1007/s10827-009-0160-8](https://doi.org/10.1007/s10827-009-0160-8) (cit. on p. [28](#)).
- [17] Maritza Mera, Diego López, Rubiel Vargas, and María Miño. “Epileptic spikes detector in pediatric EEG based on matched filters and neural networks”. In: *Brain Informatics* 7 (Dec. 2020). DOI: [10.1186/s40708-020-00106-0](https://doi.org/10.1186/s40708-020-00106-0) (cit. on p. [28](#)).
- [18] German Gomez-Herrero. “Automatic artifact removal (AAR) toolbox v1.3 (Release 09.12.2007) for MATLAB”. In: *Technology* 3 (Jan. 2007), pp. 1–23 (cit. on pp. [33](#), [35](#)).
- [19] German Gomez-Herrero, Wim Clercq, Haroon Anwar, Olga Kara (Kropotova), Karen Egiazarian, Sabine Huffel, and Wim Paesschen. “Automatic Removal of Ocular Artifacts in the EEG without an EOG Reference Channel”. In: July 2006, pp. 130–133. DOI: [10.1109/NORSIG.2006.275210](https://doi.org/10.1109/NORSIG.2006.275210) (cit. on pp. [33](#), [35](#)).
- [20] Luca Mesin, Massimo Valerio, Annette Beaumanoir, and Giorgio Capizzi. “Automatic identification of slow biphasic complexes in EEG: an effective tool to detect encephalitis”. In: *Biomedical Physics & Engineering Express* 5.4 (2019), p. 045006. DOI: [10.1088/2057-1976/ab2086](https://doi.org/10.1088/2057-1976/ab2086). URL: <https://doi.org/10.1088/2057-1976/ab2086> (cit. on p. [38](#)).
- [21] Juan Martínez, Carlos Pedreira, Matias Ison, and Rodrigo Quian. “Realistic simulation of extracellular recordings”. In: *Journal of neuroscience methods* 184 (Sept. 2009), pp. 285–93. DOI: [10.1016/j.jneumeth.2009.08.017](https://doi.org/10.1016/j.jneumeth.2009.08.017) (cit. on p. [39](#)).
- [22] Associazione Italiana per i Disturbi di Attenzione e Iperattività. URL: <https://www.aidaiassociazione.com/cose-ladhd/> (cit. on p. [47](#)).
- [23] J Millichap. “Spike and Wave EEG Abnormalities in ADHD”. In: *Pediatric Neurology Briefs* 27 (Sept. 2013), p. 72. DOI: [10.15844/pedneurbriefs-27-9-10](https://doi.org/10.15844/pedneurbriefs-27-9-10) (cit. on p. [47](#)).
- [24] John Hughes, Andrea DeLeo, and Michelle Melyn. “The Electroencephalogram in Attention Deficit–Hyperactivity Disorder: Emphasis on Epileptiform

- Discharges”. In: *Epilepsy Behavior* 1 (Aug. 2000), pp. 271–277. DOI: [10.1006/ebeh.2000.0073](https://doi.org/10.1006/ebeh.2000.0073) (cit. on p. [47](#)).
- [25] Physionet. URL: <https://physionet.org/> (cit. on pp. [49](#), [56](#)).
- [26] Antonio Quintero-Rincon, Valeria Muro, Carlos D’Giano, Jorge Prendes, and Hadj Batatia. *A novel spike-and-wave automatic detection in EEG signals*. Dec. 2019 (cit. on p. [55](#)).
- [27] Antonio Quintero-Rincon, Manuela Alanis, Valeria Muro, and Carlos D’Giano. “Spike-and-Wave detection in epileptic signals using cross-correlation and decision trees”. In: *Revista Argentina de Bioingeniería* 22 (Dec. 2018), pp. 3–6 (cit. on p. [55](#)).
- [28] Itaf Ben Slimen, Larbi Boubchir, and Hassene Seddik. “Epileptic seizure prediction based on EEG spikes detection of ictal-preictal states”. In: *Journal of Biomedical Research* 34 (May 2020), pp. 149–159. DOI: [10.7555/JBR.34.20190097](https://doi.org/10.7555/JBR.34.20190097) (cit. on p. [56](#)).

Ringrazio il Prof. Luca Mesin per il supporto e la disponibilità che, nonostante il periodo difficile, ha saputo sempre garantirmi senza far pesare il lavoro a distanza. Un grazie anche al Dott. Massimo Valerio per i consigli preziosi che hanno permesso di perfezionare il mio lavoro di tesi. Ringrazio infine la mia famiglia e miei amici che mi hanno accompagnato lungo questo percorso di studio ricco di gioie e soddisfazioni, senza mai farmi mancare niente.